UNIVERSITÀ DEGLI STUDI DI PADOVA

Engineering Faculty
Industrial Engineering Department

Master's Degree in Chemical and Industrial Processes Engineering

Brewery's residual streams exploitation through anaerobic digestion and nanocellulose production

Senior:	**Giovanni Lorenzon**
Lecturer:	**Prof. Alberto Bertucco**
Supervisor:	**Dr. Luis Cortijo Garrido**

Academic Year 2016 - 2017

Abstract

The aim of this Thesis work is to evaluate the feasibility of the implementation of a residual streams' treatment system, meant to exploit the potential of a brewery's waste production.
Breweries main byproducts consist of barley's spent grain (or Brewer's Spent Grain - BSG) and wastewater. In this work, conveniently treated mixture of BSG and wasterwater was separated by phase: the liquid part was employed to feed an anaerobic digester, while the solid fraction was used to synthesize both Cellulose Nanofibers (CNFs) and Nanocrystals (CNCs).
Quantitative and qualitative data from laboratory experience were then used to simulate process plant's performances: particular emphasis was given to the design and the computer-based simulation of the anaerobic digester.
The obtained results are encouraging and proved that high quality of both CNFs and CNCs may be reached in the final product; whereas biogas production, despite lower than similar operations, is significative though.

Contents

Chapter 1

Introduction

Nowadays growing attention is being paid to the valorization of different types of biological industrial residues: these biomasses may represent a raw material for further processing. One of the most interesting examples is represented by the BSG, a lignocellulosic residue of beer fermentation process. Many researches have shown the viability of several different applications: substrate for cultivation of microorganism [1] and enzyme production [2], source of high-added-value products such as non-cellulosic polysaccharides [3], arabino-oligoxylosides [4], hydroxycinnamic acids [5] and xylitol [6]. Moreover, recent studies are considering the production of CNFs [7] and CNCs [8] from materials similar to BSG. Nevertheless, chemical and mechanical treatments required for the syntheses of these materials are quite expensive as well as time-costing, so breweries aren't encouraged to start projects for the reuse of their residues.
This work aims at suggesting a straight-forward and cost-cutting process pathway for nanocellulosic material production; along with BSG, wastewater generated from brewery's steeping process is treated, in order to produce a suitable feed for an anaerobic digester. In this way the main byproducts in need of disposal would become a source of high added value materials and and energy.

This work is mainly divided into two stages: laboratory and simulation, which are explained below.

1.1 Laboratory

A single process pathway for BSG was designed, spotting out four different stages of the same. Particular care has been given to this part of the project: as a matter of fact, literature references of treatment processes applied to BSG showed to be extremely complex and most of all excessively expensive. The general aim of this work is to identify and evaluate a viable real-life system to implement, so worthless stages of treatment have been directly cut off after a first screening.
It was decided to perform four parallel research analysis, stopping each sample's treatment at a different stage, in order to test the performances of each output. The treatment stages were designed as follows:

- ***Stage 1 (T1):*** water and BSG are blended together, then roughly ground;
- ***Stage 2 (T2):*** the obtained mixture is set to boil;
- ***Stage 3 (T3):*** caustic soda is added and the blend is set to rest overnight;
- ***Stage 4 (T4):*** more caustic soda is added and the sample is then put in an autoclave.

Once the four samples were prepared, solid and liquid parts were separated and stored.
The solid was used to produce CNFs and CNCs: the former were prepared through mechanical microfibrillation performed with a high pressure homogenizer and preceded by catalyst-mediated oxidation; whereas the latter were obtained by acid hydrolysis.
The liquid was employed to feed four laboratory-scale batch reactors, filled with activated anaerobic sludge.
Final outputs of nanocellulose and biogas were then characterized to assess which treatment stage performed better.

1.2 Simulation

The treatment which showed to produce the highest quality output was used to design the whole waste treatment process. In particular, a computer-based model for anaerobic digestion was developed and used to fit biogas production data for the chosen best case. Once model's parameters were defined, CSTR configuration was simulated and final output for a continuous process was found. Production of CNFs and CNCs was defined accordingly.

Chapter 2

Theory

2.1 Lignocellulosic material, cellulose and nanocellulose

Wood and plants are natural biocomposites, charaterized by a hierarchically organized cellular structure. These materials are essentially made up by semicrystalline cellulose framed in microfibrils, reinforced by an amorphous matrix made of hemicellulose, lignin, waxes, extractive and trace elements [9]. Therefore lignocellulosic material is nothing but a cemented aggregate of microfibrils, as shown in Figure 2.1. [10]

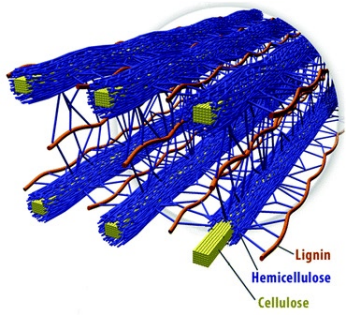

Figure 2.1: Lignocellulosic matter organization: cellulose (in green), hemicellulose (in blue) and lignin (in red).

The explained structure spans many different length scales and - as already stated - is well-organized, as it may be seen in Figure 2.2 [11]: while the whole tree is on the scale of meters, centimeters describe structures within

the cross-section, millimeters describe growth rings, tens of micrometers describe cellular anatomy, micrometers describe the layer structure within cell walls, tens of nanometers describe the configuration of cellulose microfibrils in a matrix and nanometers describe the molecular structure of cellulose, hemicellulose and lignin. [12]

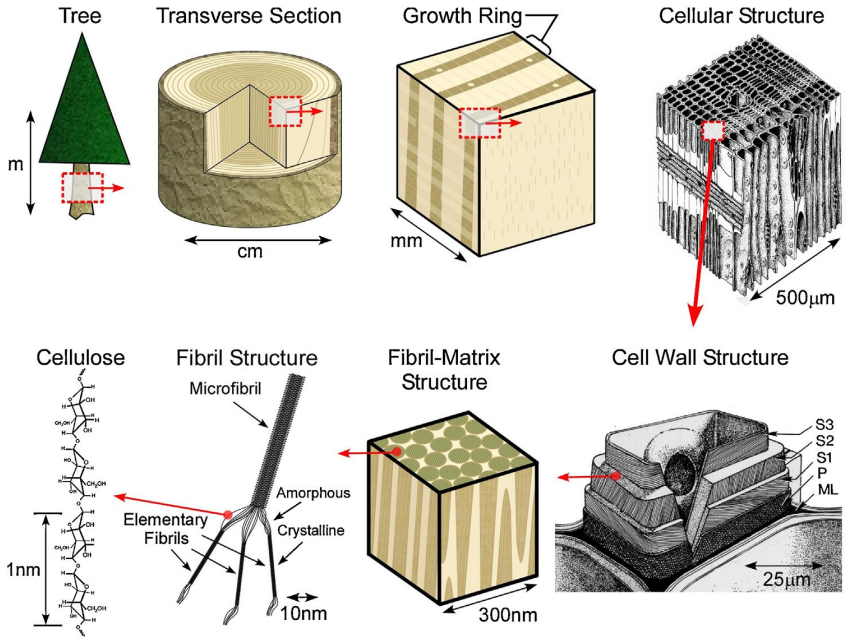

Figure 2.2: Wood's hierarchical structure.

Hence cellulose is the very fundamental "brick" of lignocellulosic material. As far as it is regarded, cellulose is the most abundant biopolymer available on the earth and shows to be fibrous, tough, water-insoluble, biodegradable, biocompatible, renewable and non toxic; but its most important attributes are its high mechanical strength and high strength-to-weight ratio.
Its chemical structure - as shown in Figure 2.3 [13] - consists of β-D-glucopyranose units, covalently linked with 1-4-glycosidic bonds; this layout gives birth to a high-molecular-weight linear homopolymer, in which every monomer unit is corkscrewed at 180° with respect to its neighbors [14]. The repeating unit of this biopolymer is cellobiose, which is a dimer of glucose. Polymerization degree for cellulose may span between $(10 \div 15) \cdot 10^3$ units, depending on the different sources [15]. Each glucopyranose is provided with hydroxyl groups, which confer to cellulose some of its main properties, such

as hydrophilicity, chirality, biodegradability etc.. Moreover, this side groups are likely to form strong hydrogen bonds with near polymer chains, behavior that lies at the basis of multi-scale fibrillated structure, hierarchical organization and crystalline regions formation [16].

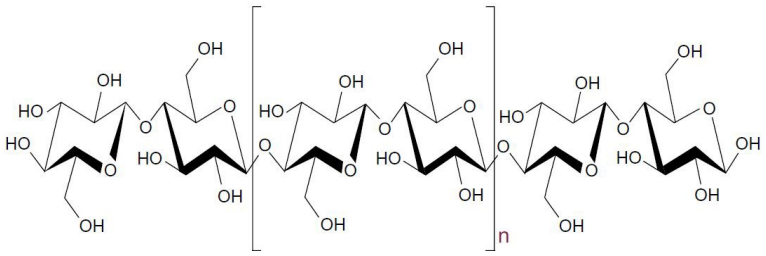

Figure 2.3: Repetitive unit of cellulose, cellubiose.

Cellulose structure and properties make this biopolymer one of the most interesting materials to be transformed into fibers and its use is widely spread (e.g. Rayon production). But in recent years a lot of attention has been drawn by cellulose nanoparticles synthesis: mechanical and chemical treatments allow to extract either the fiber bundles or the crystalline regions of the cellulose fibrils, which are characterized by impressive mechanical properties [11, 17, 18]. As a matter of fact, nanocellulose extraction eliminates all the other structural components of lignocellulosic materials, leaving only cellulose particles, which possess high modulus and low density. Crystalline cellulose has a density of $1.5 \div 1.6$ g/cm^3 and average Young's modulus around $78 \div 130$ GPa [11], while steel and Kevlar have, respectively, density of 8 and 1.45 g/cm^3, Young's modulus of 200 and 100 GPa [19, 20]. In this way, specific Young's modulus for nanoparticles ranges between $65 \div 85$ J/g (nanofibers and nanocrystals, respectively), while those of steel and Kevlar are around 25 and 50 J/g [21].

2.1.1 Cellulose nanofibers

Structure and properties

As already explained, cellulose chains inside of lignocellulosic material organize themselves in bundles, mainly because of the side hydroxyl groups which characterize the polymer. These strings are grouped together to form long and thin crystallites, which are called elementary fibrils: these struc-

tures are usually made up of a hundred of chains and are about 5 nm thick. In addition to this, elementary fibrils assemble to form microfibrils, which are $8 \div 50$ nm in diameter and the length of a few microns [22]. Eventually these microfibrils may gather together, making up even bigger layouts.
This ordered structure may be broken down using a top-down deconstruction strategy, consisting in extracting the very elements of cellulose microfibrils. This process - usually called microfibrillation - is done mechanically, by submitting slurries of cellulose fibers to high shear forces. The microfibrillated material is composed by nano-sized cellulose fibrils whose main characteristic is the extremely high aspect ratio. If the obtained fibers have a diameter whose average measures less than $50 \div 80$ nm [23], then they go under the name of cellulose nanofibers (shown in Figure 4.4 [24]) - even if common size is under 10 nm [11].

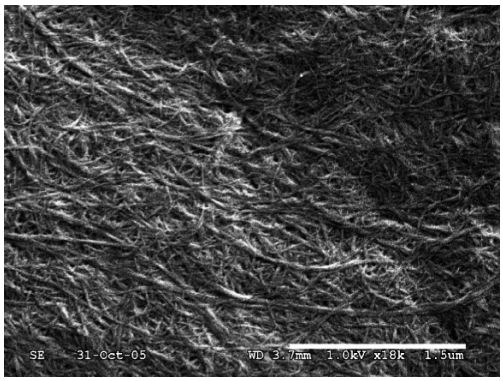

Figure 2.4: SEM image of microfibrillated cellulose film from softwood dissolving pulp.

So obtained CNFs still contain both amorphous and crystalline regions of the cellulose fibrils: this characteristic, while decreasing fibers' Young's modulus, goes with the fact that original fibrils' length hasn't been lost[1]. In this way - thanks to the very amorphous regions too - CNFs form entangled networks [26]; this structure gives nanofibers ductility and flexibility as well as a gel-like behavior in aqueous suspensions (see Figure 2.5 [16]).
This characteristic allow CNFs to be an extremely interesting material for nanocomposites production, since their flexibility, resilience and mechanical strength would enhance the composite material.

[1] At least not completely: original length of cellulose fibers could reach tens of thousands nanometers, while common CNFs' length reaches 3000 nm at most [25].

Figure 2.5: 2 % w/w microfibrillated cellulose aqueous suspension.

Mechanical fibrillation

Microfibrillation of cellulose fibers may be achieved through different strategies, but before mechanically treating raw fibers, a purification step is required.
As a matter of fact, cellulose fibers not only consist of cellulose strains, but also of hemicellulose, lignin and pectin mainly. So, the first treatment involves non-cellulosic components removal through sodium hydroxide bleaching (dewaxing with a Soxhlet apparatus might be performed too). Note that the conditions of this step have to be tailored specifically for raw material to be treated [11]. Anyway, generally speaking, the final result is lignin solubilization into bleaching solution and partial disencrustation of the cellulose microfibrils from the other components [23].
After fiber pulp is purified different types of mechanical microfibrillation may be performed, such as:

- ***High-pressure homogenization:*** $1 \div 2$ % w/w cellulose fibers' aqueous suspensions are passed through a thin slit where they are subjected to large shear forces. During homogenization dilute slurries are pumped at high pressure (around 55 MPa) and fed through a spring loaded valve assembly: as this valve opens and closes in rapid succession, fibers undergo a large pressure drop, along with shear and impact forces. This combination of stresses promotes elevated degrees of fibrillation [27];
- ***Grinding:*** cellulose fibers' slurries are processed in grinding discs grinders: they feature two non-porous ceramic disks with an adjustable

clearance between them, the surface of these elements being fitted with bars and grooves, against which fibers are subjected to repeated cyclic stress. While the upper disc is fixed, the lower one is rotated at high speed (1500 rpm); then raw material is fed into a hopper and dispersed into the discs' gap by centrifugal forces. Massive compression, shearing and rolling friction forces are applied to slurries, which are ultimately transformed into ultra-fine particles [28];

- ***Cryocrushing:*** cellulose pulp is frozen and subsequently crushed with a cast iron mortar and pestle. In doing so, ice crystals exert pressure on the cell walls and sufficient energy is expected to be provided to cause the liberation of nanofibrils [29];
- ***High-intensity ultrasonication:*** electronically generated high frequency ultrasound ($20 \div 50$ kHz) transmits its mechanical energy to the sample via an oscillating metal probe submerged into the sample. Oscillations cause localized high-pressure regions resulting in cavitation and impaction, which result in final fibrillation [30].

Pretreatments

Since cellulose fibers naturally show a tendency to flocculate, causing problems during mechanical microfibrillation, and its processing is highly energy-demanding (also because homogenization requires several passages to achieve good yield), some pretreatments may be performed on raw fibers [31]. These operations are meant to facilitate microfibrillation, reducing operation costs and improving final product quality. Well-established pretreatments are:

- ***TEMPO-mediated oxidation:*** catalytic amounts of TEMPO (2, 2, 6, 6-tetramethylpiperidine-1-oxyl) and NaBr are dissolved in cellulose fibers' suspension. Oxidation is started by adding NaClO solution as a primary oxidant: following mechanism reported in Figure 2.6 [32], efficient conversion of primary hydroxyl groups to carboxylates via aldehydes is performed. In order to proceed, the reaction is supposed to be carried out at pH values of $10 \div 11$, which are actively maintained by continuous NaOH addition. In this way microfibrillation is helped by the increased steric effect associated to carboxyl groups [32];
- ***Carboxymethylation:*** it consists in substituting hydroxyl groups of the glucopyranose monomers that make up the cellulose backbone with carboxymethyl groups ($-CH_2COOH$). This is achieved through a chemical reaction between cellulose and monochloroacetic acid in the presence of sodium hydroxide, employing isopropanol as solvent;

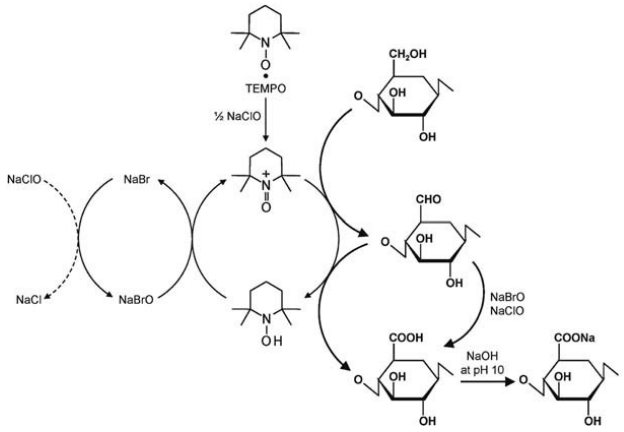

Figure 2.6: Mechanism of TEMPO-mediated oxidation pretreatment.

so, alkaline conditions increase the accessibility of fibers to chemicals thanks to swelling, allowing to exploit the high activity of internal hydroxyl groups. Once again, microfibrillation is facilitated by steric effect [33];

- ***Enzymatic pretreatment:*** enzymatic hydrolysis of cellulose is a complex mechanism, but a widely accepted pattern suggests that three different types of enzyme activities work in a synergetic way in a complete cellulase system consisting of *1)* hydrolysis of accessible intramolecular β-1,4-glucosidic bonds in cellulose chains generating oligosaccharides, *2)* release of soluble cellobiose or glucose and *3)* hydrolysis of cellobiose in order to reduce its inhibitive effect [34, 35]. Final product improvement is here achieved via partial cellulose degradation into disordered regions [24].

2.1.2 Cellulose nanocrystals

Structure and properties

Bulk cellulose consists of highly ordered, crystalline regions along with some disordered, amorphous zones in variable proportion depending on the source [36].
Cellulose fibrils could be imagined as a string of cellulose crystals, linked together by disordered segments; therefore crystalline regions act as a natural cross-linking system for the lignocellulosic matter, which gains mechanical strength [37]. Hence this domains represent a desirable material to be extracted, in order to exploit their shape and natural properties. The

extraction of these particles is similar to that applied to CNFs' synthesis, as microfibrillation is required; however, also a chemical treatment step is mandatory, in order to hydrolyze amorphous regions and leave only the crystalline ones [38]. In this way it is possible to produce whiskers or rod-shaped particles which are called cellulose nanocrystals (shown in Figure 2.7 [11]) and whose thickness may span between $3 \div 50$ nm; their length may vary between tens of nanometers up to micrometers (depending on the degree of removal of the unwanted amorphous regions) [39, 40, 41].
It has to be pointed out - though - that if chemical hydrolysis is sufficiently effective, almost all amorphous regions are dissolved; in this case the length of CNCs reaches a minimum value, associated to minimum characteristic length of the crystal, condition known as of Level-Off Degree of Polymerization (LODP) [42]. Reaching it, means obtaining a significative cut-off in degree of polymerization's values, nevertheless ensures extremely elevated levels of crystallinity for so-produced CNCs. Lengths associated to LODP are lower than those reported above and settle around hundreds of nanometers [14, 43].

Figure 2.7: TEM image of a dilute supension of cotton CNCs (crystals in the image are about 400 nm long).

An important characteristic of CNCs are their mechanical properties: although they show highly anisotropy and strongly dependance on the characteristics of the crystal domain (such as crystallinity percentage, dimensions of the crystal and presence of defects), CNCs possess stunning values for Young's modulus, which may reach 150 GPa [44]. Coupling this characteristic with the relatively low density of the material, CNCs demonstrate to be perfect charges to be used in nanocomposite materials.

Besides that, another peculiarity of CNCs is their liquid crystalline nature: under suitable conditions and at critical concentration, all asymmetric rod-like particles spontaneously form ordered structures, leading to the constitution of a chiral nematic phase (as shown in Figure 2.8 [45]) with liquid crystalline properties. In addition, CNCs show to possess birefringent nature as well, and these two characteristics offer interesting optical applications [46, 47].

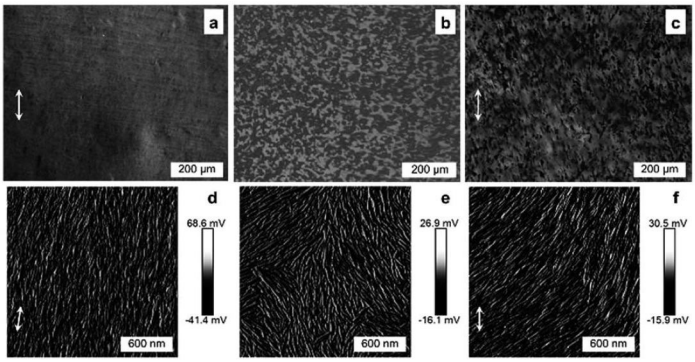

Figure 2.8: POM (a-c) and AFM (d.f) images of unaxial (a and d), nematic (b and e) and partially aligned (c and f) CNC thin films.

Acid hydrolysis[2]

Acid hydrolysis of amorphous regions of cellulose is the preferred treatment to extract CNCs from lignocellulosic material. In fact, this chemical treatment may be the only one to be applied to raw material (i.e. without any previous mechanical treatment). Nevertheless, previous grindind / milling / fibrillation ensures higher effectiveness of the whole process, also yielding to a higher number of rod-like shaped particles (instead of plate-shaped ones, deriving from non-fibrillated fibers which undergo the chemical treatment) [48].
Amorphous domains are dissolved by acid hydrolysis because crystalline regions have higher resistance to acid attack (i.e. slower hydrolysis kinetics) and so this technique leaves those domains unaltered. Typical procedure consist of four steps, here summarized:

[2]Note that for CNCs, only chemical treatments are reported, since the mechanical ones are completely alike those explained for CNFs.

1. strong acid hydrolysis of pure cellulosic material under strictly controlled conditions of temperature, time, agitation, acid concentration and acid to cellulose ratio;
2. fast dilution with water to stop reaction and reapeated washing with successive centrifugation;
3. extensive dialysis against distilled water to fully remove free acid molecules;
4. mechanical treatment (usually sonication) in order to disperse CNCs as a uniform stable suspension [49].

Sulphuric acid is typically employed, due to the fact that it reacts with the hydroxyl groups present on cellulose surface via an esterification process, allowing the grafting of anionic sulfate ester groups ($-OSO_3^-$) [50], which are randomly distributed on CNCs' surface. The presence of these negatively charged sulfate ester groups induces the formation of a negative electrostatic layer, that covers the nanocrystals and promotes their dispersion in water. The high stability of sulfuric-acid-hydrolyzed cellulose nanocrystals results therefore from an electrostatic repulsion between individual nanoparticles. The particular configuration that sulfuric acid bestows to CNCs makes it the most widely used acid for cellulosic materials' hydrolysis, but also hydrochloric acid, nitric acid and some organic acids have been effectively used [11].

2.2 Anaerobic digestion

Anaerobic Digestion (AD) is one of the main processes used for sludge stabilization. It is widely employed with streams such as manure, industrial wastewaters and organic fraction of municipal solid waste. Generally, it is regarded as a complex process, mainly because digestion itself is based on a reduction process consisting of a number of biochemical reactions, taking place under anoxic conditions [51]. However, one can distinguish four steps involved in this process: hydrolysis, acidogenesis, acetogenesis, and methanogenesis. But this is not the only possible classification, as also the bacterial groups involved in these stages may be categorized: fermentative bacteria regulate both hydrolysis and acidogenesis steps, while acetogenic and methanogenic bacteria control acidogenesis and methanogenesis, respectively. A simple schematic of the the overall process is shown in Figure 2.9 [52]

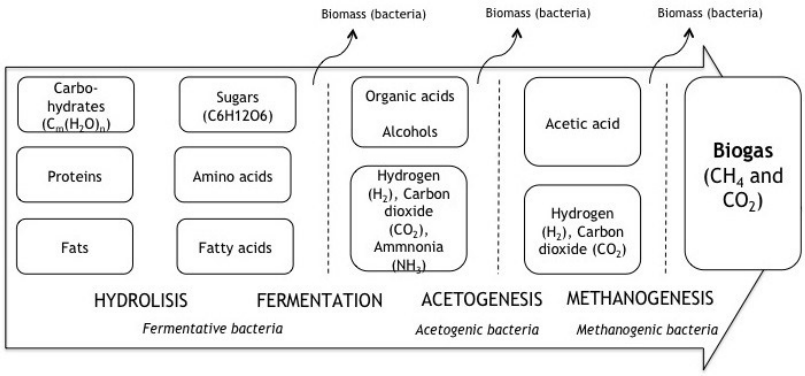

Figure 2.9: Schematic of anaerobic digestion's main features and stages.

First, complex polymeric materials such as polysaccharides, proteins and lipids are hydrolyzed to soluble products by extracellular enzymes; this is necessary for the substrate in order to reach the required size to allow its transport across bacterial cell membranes. These relatively simple, soluble compounds are fermented or anaerobically oxidized to volatile (short-chain) fatty acids (VFAs), alcohols, carbon dioxide, hydrogen and ammonia. VFAs (except for acetate) are converted into acetate, hydrogen gas and carbon dioxide. Lastly, methanogenic bacteria produce methane, either from acetate or from hydrogen and carbon dioxide [53].

Anaerobic digestion shows the advantage of producing small amounts of sludge (with respect to aerobic digestion, which requires more nutrients and energy as well), while the generated biogas can be used as an energy source. Unfortunately, anaerobic systems can be unstable due to feed overload or to the presence of inhibitors (e.g. high concentration of VFA, ammonia or hydrogen), or even by inadequate temperature control [54]. So, AD's performance depends on several parameters. Moreover, since different groups of microorganism are involved in biogas production, suitable operation conditions have to match the needs of all those group; thus it is necessary to define an adequate balance with extreme accuracy. Some fundamental parameters are [51, 55, 56, 57]:

- ***pH:*** a neutral pH is favorable for biogas production, since most of the methanogens grow inside a pH range of $6.7 \div 7.5$;
- ***temperature:*** most of the acid forming microorganisms grow under mesophilic ($\sim$37 °C) conditions; however, for methanogens, a higher temperature ($\sim$55 °C) is favorable;

- ***mixing:*** it is essential for biogas production, as too much mixing stresses the microorganisms and without mixing foaming occurs;
- ***substrate:*** it must possess good biodegradability towards hydrolytic bacteria; complex macromolecules such as lignin may increase the hydrogen concentration too much, while slowing the acetoclastic - methanogenic process;
- ***C/N ratio:*** the balance of carbon sources with other nutrients such as nitrogen, phosphorus and sulfur is fundamental; for instance, carbon/nitrogen ratio should be around 16:1 ÷ 25:1. Uncontrolled increase or decrease in the carbon/nitrogen ratio affects biogas production, because that would stand, respectively, for an excess or a lack of nutrients;
- ***hydraulic Retention Time (HRT):*** methane-producing microorganisms grow slowly, with a doubling time of around 5 ÷ 16 d; therefore, the HRT should be at least of 5 ÷ 10 d.

2.2.1 Mechanism

Hydrolysis

During hydrolysis, polymerized and mostly insoluble organic compounds such as carbohydrates, proteins and fats are decomposed into soluble monomers and dimers (i.e. monosaccharides, amino acids and fatty acids). This stage of anaerobic digestion passes through extracellular enzymes from the group of hydrolases (amylases, proteases and lipases) synthesized by specific strains of hydrolytic-fermentative bacteria [58, 59]. Hydrolysis of hardly decomposable polymers, for instance lignocellulosic materials or complex phenolic matter, is a stage which limits the rate of wastes digestion.
During solid wastes digestion, only 50 % of organic compounds is supposed to undergo biodegradation; the remaining part of the compounds stays unaltered in its primary state, mainly because of the lack of enzymes participating in their degradation.
The overall rate of hydrolysis depends on parameters such as size of particles, pH, production of enzymes, diffusion and adsorption of enzymes on the particles of wastes [60, 61].

Acidogenesis

During this stage, the acidifying bacteria convert water-soluble chemical substances (i.e. hydrolysis products) to short-chain organic acids (formic,

acetic, propionic, butyric and pentanoic), alcohols (methanol, ethanol), aldehydes, carbon dioxide and hydrogen [56]. The basic pathway of methane production passes through acetates, CO_2 and H_2, whereas other acidogenesis products must be converted by hydrogen producing bacteria during acetogenesis.
Accumulation of compounds such as lactate, ethanol, propionate, butyrate and higher VFAs is the bacterial response to an increase in hydrogen concentration in the solution. Moreover, also ammonia and hydrogen sulfide are produced during this stage (responsible for the unpleasant smell) [62, 63, 64].

Acetogenesis

Throughout this stage, the acetate bacteria convert the acid phase products into acetates and hydrogen, that may be used by methanogenic bacteria [65]. As a result of acetogenesis, significative amount of hydrogen is released, which exhibits toxic effects on the same microorganisms that carries out this process. Therefore, acetogenic bacteria are required to establish a symbiosis with autotrophic methane-producing and hydrogen-consuming bacteria [65, 66].
Acetogenesis is fundamental for the total efficiency of biogas production, because approximately 70 % of methane comes from acetates reduction. As a consequence, acetates are a key intermediate component in the process of anaerobic digestion. It's worth noting that, during acetogenesis stage, approximately 25 % of acetates are formed and approximately 11 % of hydrogen is produced [65].

Methanogenesis

This stage consists in the production of methane by methanogenic bacteria; its synthesis comes from the degradation of the products of the previous stages, that are acetic acid, CO_2 and H_2, mainly. Despite the fact that only few methanogenic bacteria are heterotrophic (i.e. acetoclastic), the vast majority of methane arising in this stage results from acetic acid degradation [67]. Only 30 % of methane produced comes from CO_2 reduction carried out by autotrophic methane bacteria.
During the process, H_2 is finally consumed, allowing for good development of acid bacteria; their flourishing gives rise to increased VFAs in acidification stage and consequently a lower production of H_2 in acetogenic stage. Such configuration may cause high CO_2 production, because of the lack of available H_2 to react with [68, 69].

2.2.2 Kinetics and modeling

Due to the significative instability that may arise from the operation of AD reactors, many studies have been performed to identify the key parameters influencing the process, in order to develop reliable models. In the last decades, several models have been published, with an increasing precision in considering all the complex mechanisms involved in anaerobic digestion. Nevertheless the fundamental basis of all these works can be traced back to two fundamental kinetics: the hydrolysis and microbial growth ones [70].

Hydrolysis

Essentially, hydrolysis is a combination of two processes, solubilization of insoluble particle matter and biological decomposition of organic polymers. Extracellular enzymes are in charge of this process, but this is not necessarily an enzymatic-catalyzed step, since hydrolysis may be caused by physicochemical reactions as well.
The whole process is extremely difficult to describe with a trustworthy kinetics, giving to the many parameters to be accounted for, such as particle size, pH, production of enzymes, diffusion and adsorption of enzymes to particles. Anyhow, hydrolysis of organic polymers is often described through a first-order kinetics, since its activity is not directly related to that of the bacterial population [53]. Moreover it has been found that a first-order function may be more appropriated for complex, heterogeneous substrates (while for homogeneous ones other modifications are more effective) [71].
Typical equation for the proposed model is:

$$r_S = K_h \cdot S \tag{2.1}$$

Where r_S is the rate with which substrate is transformed into available matter, K_h is the specific hydrolytic constant and S is the concentration of polymerized substrate.

Microbial growth

According to Pavlostathis et al. (2004) [53], cell growth generally involves a respiratory or a fermentative conversion of the substrate, which leads to the release of some products and energy (in the form of ATP). The energy produced in this stage (catabolism) is then employed both to synthesize new cells and maintain the old ones (anabolism). The sum of the two processes gives the overall metabolism of the bacteria.

$Catabolism$	$Substrate \rightarrow Microbialproducts + Energy$
$Anabolism$	$Substrate + Energy \rightarrow Microorganisms$
$Metabolism$	$Substrate \rightarrow Microbialproducts + Microorganisms$

The ration between the concentration of produced cells and the substrate permits the calculation of the the biomass yield factor:

$$Y_{X/S} = \frac{\Delta X}{\Delta S} \tag{2.2}$$

Where X stands for the biomass concentration. One of anaerobic degradation's common feature is the fact that it possesses low biomass yield factors compared to aerobic, as $Y_{X/S}$ generally lies between $0.05 \div 0.2$ grams of biomass per gram of substrate.
In addition, product yield factor describes the ratio between microbial products and consumed substrate:

$$Y_{P/S} = \frac{\Delta P}{\Delta S} \tag{2.3}$$

The kinetic growth of the bacterial population is usually described through a Monod equation:

$$r_X = \mu(S, X) \cdot X \tag{2.4}$$

Where r_X is the bacterial growth rate and $\mu(S, X)$ the specific growth rate of the microorganism. Monod proposed to express μ as:

$$\mu = \frac{\mu_{max} \cdot S}{K_S + S} \tag{2.5}$$

Where μ_{max} is the maximum specific growth rate, reached only when the concentration of the substrate is in excess (i.e. $S \gg K_S$), while K_S stands for the saturation constant, that is the value of substrate's concentration at which the growth rate is half of its maximum.
Combining the two expressions, it is possible to write:

$$r_X = \frac{\mu_{max} \cdot S}{K_S + S} \cdot X \tag{2.6}$$

Note that another parameter is usually added to this form, which accounts for the decrease of the biomass concentration due to endogenous respiration and cell lysis, so that:

$$r_X = \frac{\mu_{max} \cdot S}{K_S + S} \cdot X - b \cdot X \tag{2.7}$$

Where b is the specific decay coefficient for the microorganism.
Lastly, substrate consumption has to be addressed, which is directly related to bacterial growth rate through the biomass yield factor. As a matter of fact, its consumption is represented by the equation:

$$r_S = \frac{1}{Y_{X/S}} \cdot r_X = \frac{1}{Y_{X/S}} \cdot \frac{\mu_{max} \cdot S}{K_S + S} \cdot X \tag{2.8}$$

Chapter 3

Materials and methods

3.1 Laboratory

3.1.1 BSG treatments

Raw BSG from "La Cibeles" hand-crafted brewery (Madrid) has been treated according to a four-stage pathway:

- ***Stage I (T1):*** BSG was diluted with distilled water until reaching 12.71 % w/w concentration and then ground with a kitchen-mixer for 150 s;
- ***Stage II (T2):*** ground mixture was set to boil at 110 °C for 2 h;
- ***Stage III (T3):*** 35 % w/w soda aqueous solution was added to reach 2 % w_{SODA}/w_{BSG} concentration and let at rest for a timespan of 16 h;
- ***Stage IV (T4):*** further soda was added until a concentration of 12 % w_{SODA}/w_{BSG}; then sample was sealed and put into an autoclave at 121 °C for 1 h;

Samples from the four passages were collected and put into a centrifuge at 4000 g for 10 min in order to collect and store pure, undiluted liquor. After that, several passages of dilution and centrifugation were performed until transparent water came out of the centrifuged samples.

3.1.2 BSG characterization

Both raw and treated BSG have been characterized for their components; seven main contributions have been investigated, which are listed below:

- ***Lignin*** was determined following Laboratory Analytical Procedure (LAP) "Determination of structural carbohydrates and lignin in biomass" by National Renewable Energy Laboratory (NREL) [72]: 300 mg of dry, extractive-free BSG sample were placed in a 30 °C water bath and hydrolysed with 3 mL of 72 % w/w sulphuric acid (agitation was provided with stir rod every 8 min), for a total timespan of 60 min. Upon completion of the hydrolysis, 84 mL of distilled water were added to the sample, diluting acid concentrations to 4 % w/w; hydrolysed matter was then sealed and placed into an autoclave for 1 h at 121 °C. The obtained final sample was vacuum-filtered with known-weight glass-fiber crucibles, which were then oven-dried at 105 °C for 12 h and ultimately placed in a muffle furnace at 575 °C for 24 h (measuring the weight before and after each passage). Hydrolysis liquor from filtering step was placed into a UV-visible spectrophotometer: using distilled water as a background, absorbance at 240 nm was measured on diluted sample, until its value fell in the range $0.7 \div 1.0$. Lastly acid insoluble lignin (AIL) and acid soluble lignin (ASL) were calculated thanks to the following expressions:

$$\begin{aligned} \%\ AIR &= \frac{Weight_{oven-dried\ crucible} - Weight_{crucible}}{ODW} \cdot 100 \\ \%\ AIL &= \%\ AIR - \frac{Weight_{muffled-dried\ crucible} - Weight_{crucible}}{ODW} \cdot 100 \\ \%\ ASL &= \frac{ABS_{UV} \cdot Volume \cdot Dilution}{\varepsilon \cdot ODW \cdot Pathlength} \cdot 100 \end{aligned} \tag{3.1}$$

  Where AIR stands for Acid Insoluble Residue, ODW for Oven Dry Weight (i.e. dry weight of the initial sample), $Volume$ for the sample volume (86.73 mL), ε for absorptivity of the biomass at specific wavelength (25 L/g cm) and $Pathlength$ for the length of the spectrophotometer cell in centimeters (1 cm). Naturally, final conversion considering the amount of the extractives (previously removed for this analysis) has to be performed;
- ***Proteins*** were determined by direct correlation with total nitrogen present in BSG samples. A conversion factor of 4.96 [73] was employed to convert nitrogen content data from combustion micro-elemental analysis;
- ***Fatty acids*** were estimated by difference before and after extraction with dichloroethane in a Soxhlet system: 3 g of dry BSG was placed in the extraction cup of the apparatus, while reboiler flask was filled

with 200 mL of dichloroethane. Extraction was performed for a total of 24 h (∼120 cycles) [74];
- ***Cellulose*** was measured by difference from the other investigated components (thus it's worth noting that its value includes hemicellulose as well);
- ***Sugars*** were measured employing standard kit from Megazyme [75];
- ***Starch*** was measured employing standard kit from Sigma-Aldrich [76];
- ***Ashes*** were measured by difference between dry BSG and a BSG sample placed in a muffle furnace at 575 °C for a total amount of time of 24 h;

3.1.3 Liquor characterization

Liquor from the BSG treatment stage was characterized in order to define organic and inorganic carbon content, nitrogen content and Chemical Oxygen Demand (COD). As far as the first two are regarded, measurements have been performed with Analitik-Jena Multi N/C® 3100 TOC/TN_b liquid analyzer; whereas COD measurements have been performed with Metrohm MATi 12 system for automated COD determination.

3.1.4 CNFs synthesis

CNFs synthesis consisted in a two step preparation: a TEMPO-mediated oxidative pretreament followed by mechanical high-pressure homogenization.
Oxidation was performed employing proportions of 0.016 g of TEMPO, 0.1 g of NaBr and 10 mmol of NaClO per gram of treated BSG. 1 % w/w aqueous solution of BSG was mixed with required amounts of TEMPO and NaBr, then stirred at high-velocity for 30 min; after slow addition of NaClO (activator of the reaction), the oxidation batch was maintained at a constant pH value of 10 by continuous addition of 1 M NaOH aqueous solution, until constant pH.
After catalytic oxidation, samples were repeatedly rinsed with distilled water, for several cycles of dilution and filtration, through a stich (until stable pH value was reached). High-pressure homogenization was then performed, employing a laboratory homogenizer PANDA PLUS 2000 manufactured by GEA Niro Soavi, for a total number of 6 cycles of homogenization.

3.1.5 CNFs characterization

Characterization technique applied to CNFs follow:

- ***Fibrillation yield*** calculation, achieved by measuring supernatant's consistency of a 0,1 % w/w CNFs aqueous suspension centrifuged at 4500 g for 20 min: ratio with non-centrifuged sample's consistency gave the yield;
- ***Transmittance*** measurement of 0,1 % w/w CNFs aqueous suspension between 400 ÷ 800 nm;
- ***SEM imaging***.

3.1.6 CNCs synthesis

First passage in CNCs production was to completely dry and mill the samples coming from the treatment step. After that, proper CNCs synthesis was achieved upon amorphous cellulose hydrolysis: a water bath at 55 °C was prepared and the sample was put inside; then, 60 % w/w sulphuric acid aqueous solution was added with the proportion of 13,5 $\mathrm{mL}_{H_2SO_4}/\mathrm{g}_{BSG}$to start hydrolysis. Continuous stirring was achieved with a PTFE, two-blade impeller, for a total timespan of 1.5 h. Then hydrolysis was blocked by adding distilled water, thus cutting acid concentration tenfold.
Cleaning was performed through centrifugation and further dialytic treatment against pure water, until a stable pH value of 6,5 was reached.

3.1.7 CNCs characterization

Characterization techniques applied to CNCs were:

- ***Degree of polymerization (DP)*** was determined from intrinsic viscosity ($[\eta]$) according to Heriksson et al. equation [24]:

$$[\eta] = 0.42 \cdot PD, \qquad PD < 950 \tag{3.2}$$

  $[\eta]$ was measured by the method of dissolving cellulose in cupri-ethyenediamine (CED) solution, according to ISO 5351;
- ***X-ray diffraction (XRD)*** spectra were obtained using a Philips X'Pert MPD X-Ray diffractometer with an autodivergent slit fitted with a graphite monocromator using Cu-Kα radiation operated at 45 kV and 40 mA. The XRD patterns were recorded from 3 to 80° at a scanning speed of 1.5°/min. Crystallinity index (Cr.I) was determined using Segal's method [77], employing the reported equation:

$$Cr.I(\%) = \frac{I_{002} - I_{am}}{I_{002}} \cdot 100 \tag{3.3}$$

Where I_{002} is the intensity of the 002 plane at $2\theta = 22.5°$ and I_{am} is the intensity of the amorphous scatter at $2\theta = 18°$;
- ***SEM imaging***.

3.1.8 Anaerobic digestion

Liquor stored from the BSG treatment stage was employed as feed for a set of four anaerobic digestors: 250 mL capacity laboratory bottles were employed as reactors and kept into a heated stove at 35 °C. First, they were filled with active anaerobic sludge from another available digester and fed with T1 liquor for a period of two weeks. These reactors were operated in a semi-batch way, where the feed was discontinuously fed and the produced gas could flew outside of the bottles into bags. After that, mentioned liquors were fed to the reactors (one type for each reactor) and biogas production measured daily, employing a MilliGascounter MGC-1 PMMA manufactured by RITTER Apparatebau.

3.2 Simulation

3.2.1 Model structure

The simulation of an anaerobic digester was designed in the Matlab environment. It's worth noting that the model developed was quite simple. Its structure was built in a simplified manner, adopting a bottom-up approach and starting from the very basic kinetics of anaerobic digestion. The main assumptions are:

- ***Monod's*** equation for anaerobic bacterial growth was used as the only kinetics for microorganisms' growth rate (see Paragraph 2.2.2);
- ***Hydrolysis*** was assumed to be a first-order mechanism;
- ***Inhibition*** of bacterial metabolism was neglected.

The three main groups of bacteria involved in anaerobic digestion (acidogenic, acetogenic and methanogenic) have been accounted for, based on biomass yield factor approach to assess mutual variation of microorganism and substrate. Since each group may feed on different types of substrate,

the expressions for growth rate follow:

$$\mu_i = \frac{\mu_{max} \cdot \sum_j^{sub} S_j}{K_S + \sum_j^{sub} S_j} \qquad (3.4)$$
$$r_{X_i} = \mu_i \cdot X_i - b_i \cdot X_i$$

Where i stands for the bacterial group and j for one of the substrates the same group feeds on.
Therefore, for each substrate consumed, the following expression holds:

$$r_{S_j} = \frac{\mu_i \cdot X_i}{Y_{X_i/S_j}} \cdot \frac{S_j}{\sum_j^{sub} S_j} \qquad (3.5)$$

In this way, the consumption's velocity of a substrate results dependant on its own fraction among all the possible substrates a population can feed on[1].

Although initial available substrate was well-known (from experimental composition analysis), a variety of microbial products might be produced from a single substrate. Therefore it has been necessary to define all the chemical reactions involved in the process, in order to outline the involved species as well. An exhaustive list of all the reactions is reported in Table 3.1,from which it is possible to see that hydrolysis reactions have been simplified in order to account for the main substrate-product couples only. In addition, glucose decomposition has been divided into different pathways (percentage values describe likeliness of the reaction to take place), to account for the distribution of products it may give. Finally, aminoacids' products has been averaged on a mass basis, given that a single reaction is impossible to be build because of the great variety of aminoacids.

The last problem to be addressed is that, contrarily to what happens for microorganism and substrate, the relationship between microbial products and substrate mutual variation isn't well defined in literature (i.e. $Y_{P/S}$ data aren't available as happens for those of $Y_{X/S}$). Consequently, the correlation between these quantities has been derived from the chosen stoichiometric

[1]Note that, without this contribution, each substrate would be consumed at a rate which depends on the sum of all the substrates, thus way higher.

coefficients, as reported below:

$$Y_{P_k/S_j} = \frac{\nu_{Pk}}{\nu_{S_j}} \cdot \frac{PM_{P_k}}{PM_{S_j}} \tag{3.6}$$

Therefore, microbial products' rate of production is:

$$r_{P_j} = Y_{P_k/S_j} \cdot r_{S_j} \tag{3.7}$$

Table 3.1: Main reactions for substrates and microbial products in anaerobic digestion.

SUBSTRATE	REACTION[78]
	HYDROLYSIS
Cellulose	$CELL \rightarrow GLUC$
Protein	$PROT \rightarrow 50 \cdot AMIN$
Fat	$FAT \rightarrow 3 \cdot LCFA$
Lignin	$14 \cdot LIGN \rightarrow 23 \cdot PHEN$
	ACIDOGENESIS
Glucose (50%)	$GLUC + 2 \cdot H_2O \rightarrow 2 \cdot ACET + 2 \cdot CO_2 + 4 \cdot H_2$
Glucose (35%)	$3 \cdot GLUC \rightarrow 4 \cdot PROP + 2 \cdot ACET + 2 \cdot CO_2 + 2 \cdot H_2O$
Glucose (15%)	$GLUC \rightarrow VALE + 2 \cdot CO_2 + H_2$
Aminoacids	$1kg\ AMIN \rightarrow 0.42kg\ ACET + 0.27kg\ BUTY + 0.24kg\ VALE + 0.06kg\ H_2$
	ACETOGENESIS
Valerate	$VALE + 2 \cdot H_2O \rightarrow PROP + ACET + H_2$
Butyrate	$BUTY + 2 \cdot H_2O \rightarrow 2 \cdot ACET + 2 \cdot H_2$
Propionate	$2 \cdot PROP + 2 \cdot H_2O \rightarrow 3 \cdot ACET + 2 \cdot H_2$
LCFA[2]	$LCFA + 14 \cdot H_2O \rightarrow 8 \cdot ACET + 14 \cdot H_2$
Phenol	$2 \cdot PHEN + 12 \cdot H_2O \rightarrow 5 \cdot ACET + 2 \cdot CO_2 + 8 \cdot H_2$
	METHANOGENESIS
Acetate	$ACET \rightarrow METH + CO_2$
CO_2/H_2	$CO_2 + 4 \cdot H_2 \rightarrow METH + 2 \cdot H_2O$

3.2.2 Fitting technique

Model's parameters fitting was performed with the help of an algorithm which simulated the annealing process [79]. Its working principle is based

[1]LCFA may have several lengths, but in this study is approximated with C_{16} (i.e. palmitic acid).

on a fictitious temperature parameter, which reflects the system's "degree of excitement".
First of all, parameters set was randomly generated inside of a user-imposed range, in the middle of which the literature values laid. Objective function's value (FOB, i.e. the sum of the quadratic errors) was then calculated with the same set. After that, the values of the parameters were translated into four-digit Grey's code scale (to ensure smoothness between iterations) and randomly modified: one of the four available digits per parameter was switched (i.e. from 0 to 1 and viceversa), resulting in a shift of the parameter's value depending on its formerly assigned range of variation. Modified set was then used to calculate the new FOB, which was compared to the previous one. At this point, the new value of FOB (and of parameters as well) might be accepted or rejected: the acceptance criteria was function of both the FOB's value (lower FOB is preferably accepted) and the fictitious temperature. High values of temperature might have implied the acceptance of parameters set associated to higher FOB (with respect to the previous step). Therefore it was assigned a high initial value to the temperature, in order to allow the acceptance of parameters set which might be far from local minimum, but possibly closer to an absolute minimum. Temperature was then decreased at each step, as to transform final iterations of the algorithm in a simple local minimum search.
Parameters values obtained from this algorithm were eventually employed in a more accurate local minimum search routine to find final values for the parameters.

Chapter 4

Laboratory

In this chapter the results collected from the experiments performed in laboratory are reported. Throughout this section both quantitative and qualitative aspects of the outputs will be analyzed and discussed, in order to precisely depict the characteristics of each scenario. The chapter consists of five parts, related to preliminary characterization of untreated BSG, subsequent characterization after treatment, CNFs production, CNCs production and wastewater treatment, respectively.

4.1 Preliminary characterization

The first step of the laboratory work has been to analyze raw BSG from brewery in order to assess the amount of the main biological macromolecules; a detection limit of 1% has been set: below that value any category would be excluded. Moreover, note that the amount of cellulose has been assessed by difference, through the estimation of all the other biological macromolecules; that means that the so-obtained values include both cellulose and hemicellulose.

The results for unprocessed BSG reported in Table 4.1 are consistent with the composition of a common bran, rich in lignin, cellulose, proteins and fatty acids [80, 81, 82]; whereas starch and sugars have been completely removed during the previous fermentation step of barley. Besides it is interesting to point out that the ashes are mainly made up by silicates and silica compounds (as shown in Appendix A).

Table 4.1: Untreated BSG composition.

MACROCOMPONENT	AVERAGE CONTENT (% w/w)
Lignin	21.30 ± 0.17
Proteins	22.43 ± 2.98
Fatty acids	19.99 ± 1.33
Cellulose	32.64 ± 4.60
Sugars	*undetectable*
Starch	*undetectable*
Ashes	3.64 ± 0.12

Apart from composition measures, untreated BSG has been analyzed through SEM to depict its three-dimensional structure. As shown in Figure 4.1 the structure is mainly made up by toothed fibrils tightly connected, which show a diameter of few micrometers and a length which could span from hundreds micrometers to millimeters.

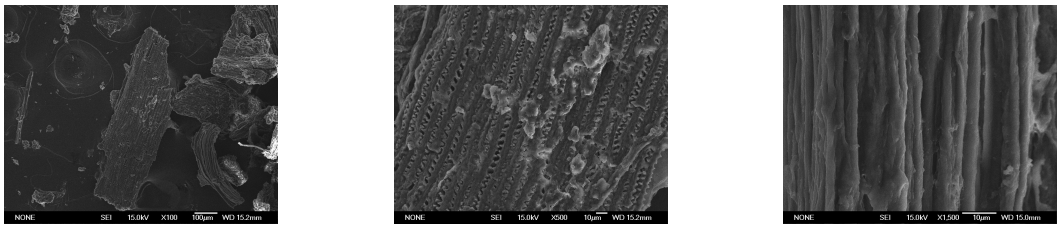

(a) Zoom x100 (b) Zoom x500 (c) Zoom x1500

Figure 4.1: SEM images of untreated BSG at different degrees of magnification.

4.2 Post-treatment characterization

The same analyses performed on untreated BSG have been repeated on the solid produced by different treatments, after complete liquid removal and drying. In Figure 4.2 the composition of the same main components as before are represented after each treatment stage (in Appendix A the corresponding table is reported). It is clear that the first two steps of treatment do not significantly affect the composition's distribution; on the other hand, the third and fourth ones show significant decrease in fatty acids and pro-

teins, along with quite a considerable loss of lignin. As a consequence, the treated BSG is rich in cellulose, thus suitable for nanocellulose production.

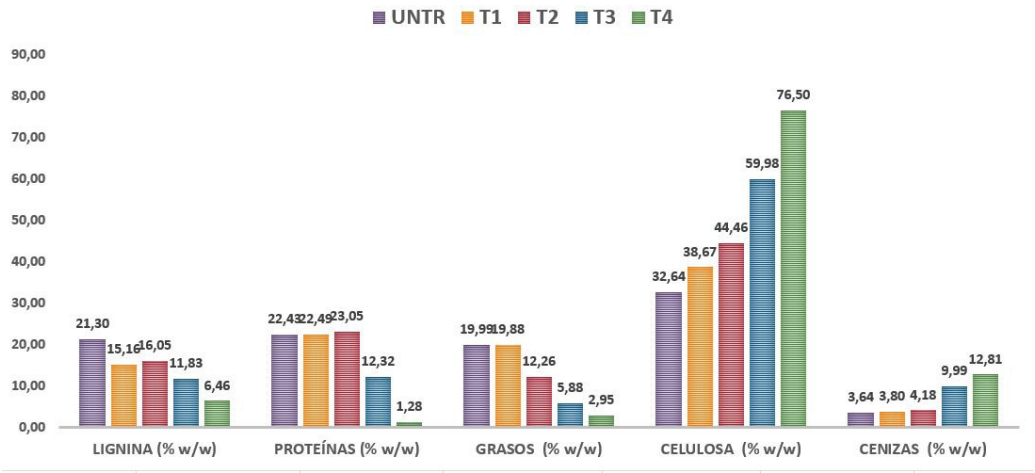

Figure 4.2: Untreated and treated BSG composition.

The variation of the composition is mostly due to the fact that water and soda dissolve a consistent amount of the BSG in the liquid phase. Apparently, the grinding process allows a better dissolution.
In Table 4.2 the solid yields of the treatments are reported, i.e. the amount of dry solid left after the treatment (the undissolved solid). The table shows the first and one of the most important problems, which is the extremely low yield of the most intense treatment (i.e. last stage); the solid output would be perfect to be processed for nanocellulose production, but the ultimate amount of product to be sold would be a smaller fraction of the initial raw material.

Table 4.2: Solid yields for treated BSG.

TREATMENT	SOLID YIELD (% w/w)
T1	92.59 ± 1.81
T2	91.98 ± 1.84
T3	52.40 ± 4.71
T4	15.03 ± 0.59

Another important consideration is the aspect of the obtained solid: it is possible to notice a progressive color loss and particle dimension decrease as the treatments proceed further on. The first effect is due to the lignin removal, while the second one depends on the strong basic environment which attacks the BSG and considerably reduces its initial particle size. This effect results to be quite important for further processing for both CNCs and CNFs: acid hydrolysis and TEMPO-mediated oxidation, respectively, will enhance their yields.

As far as the liquid part is concerned, its composition significatively varies depending on the applied treatment, as shown in Table 4.3: the total COD increases by a factor 5, while the total carbon content by a factor 10. The nitrogen content increases as well, since the proteins are degraded by the sodium chloride, which dissolves them into the liquid phase.

Table 4.3: COD, carbon and nitrogen content of liquor collected after the treatments.

TREATMENT	CARBON (g/L)		NITROGEN (mg/L)	COD (g/L)
	ORGANIC	INORGANIC		
T1	6.40 ± 0.40	0.00 ± 0.00	862.3 ± 62.5	17.046 ± 1.500
T2	8.24 ± 0.80	0.00 ± 0.00	1078.6 ± 74.4	22.344 ± 2.439
T3	20.78 ± 1.94	0.63 ± 0.02	2320.0 ± 170.9	50.178 ± 5.865
T4	55.59 ± 3.47	11.81 ± 1.29	5566.7 ± 540.4	88.673 ± 5.988

The obtained values for COD are extremely high in the last stage of treatment, but the amount of liquid collected at this point is quite small compared to the wastewater production linked to the same amount of treated BSG (more than one order of magnitude).

4.3 CNFs synthesis

The synthesis of CNFs was not possible for all the four analyzed stages of treatment: for the first two, the homogenization steps resulted impossible to perform, mainly because of the particle size. Therefore only two types of sample have been characterized (T3 and T4), for which transmittance at 800 nm and non-centrifuged/supernatant density ratio have been calculated.
As reported in Table 4.4, a strong difference between the quality of the two outputs is highlighted, which scores perfect values for the last stage of treatment.

Table 4.4: Ratio between non-centrifuged sample and supernatant of the centrifuged one for CNFs 0.1 % w/w aqueous solution.

TREATMENT	ρ_{unc}/ρ_{sup} (%)
T3	20.07 ± 4.57
T4	100.15 ± 4.96

Validation of these results comes from the analysis of the transmittance, shown in Table 4.5: the reported value for the same stage of treatments is perfectly consistent with high quality CNFs output [7, 83]. In Appendix A transmittance plot for length sweep are reported as a function of the wave length).

Table 4.5: Transmittance values at 800 nm for CNFs 0.1 % w/w aqueous solution.

TREATMENT	TRANSMITTANCE (%)
T3	31.94 ± 1.24
T4	83.12 ± 0.22

It is possible to spot the difference in quality of the two samples observing their very colors: as shown in Figure 4.3, the T4 sample (on the left) is completely white, which means that the product has achieved high purity in cellulose. In addition, the homogeneous opacity shows the stability of the suspension, which stands for cellulose nanofibers of perfect homogeneous dimension. Whereas T3 sample (on the right) shows a yellowish color, indicating that a certain amount of lignin stuck to the fibers.

Another important information is the yield of the CNFs' production, which is reported in Table 4.6: data underline how low the T4 CNFs synthesis' yield is, which ultimately leads to a small amount of final product. Justification of this, has to be traced back to both the TEMPO-mediated oxidation step, which dissolves an additional part of the solid, and the filtering step, which eliminates all the particles whose size lies below ~ 50 nm (i.e. a part that might be of a considerable amount for T4 sample).

The quality of the fibers has been assessed through AFM as well, in order to investigate the shape and the average fiber size. Figure 4.4 reports the scans

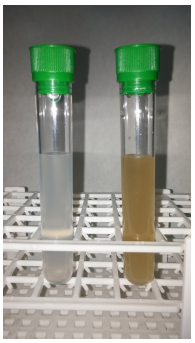

Figure 4.3: T3 (right) and T4 (left) samples of CNFs 0.1 % w/w aq. solution.

Table 4.6: CNFs production yields.

TREATMENT	YIELD (% w/w)
T3	46.98 ± 4.87
T4	34.02 ± 3.08

for CNFs 0.0001% w/w aqueous solution with dispersant, from which conclusions can be drawn: the first one regards the length of the fibers, which is quite smaller for T4 output, possibly due to the strong concentration of soda associated to the preliminary treatment. The second one regards the amount of fibers observed in the area of the scan, which are way fewer in T3 image; this is probaly so because of the non-homogeneous particle size distribution, meaning that only a tiny part of the total fiber amount has a dimension similar to the one observed with AFM, while the rest shows higher values. Precise values of length, thickness and aspect ratio are reported in Table 4.7.

Table 4.7: Length, thickness and aspect ratio for CNFs.

TREATMENT	LENGTH (nm)	WIDTH (nm)	ASPECT RATIO (l/w)
T3	1101 ± 160	3 ± 1	~ 367
T4	160 ± 45	3 ± 1	~ 53

The results above are quite important in order to evaluate which stage of treatment represents the optimum between production cost and sale profit: T3 fibers prove to possess higher length (consistent with CNFs average literature values, that lies around $800 \div 2000$ nm [7, 25]), which is an important

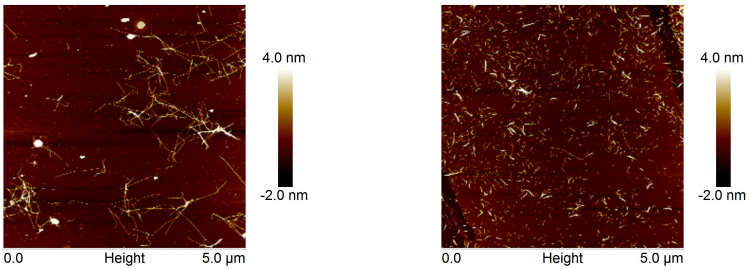

(a) T3 (b) T4

Figure 4.4: AFM images of CNFs 0.0001% w/w aq. solution.

characteristic for mechanical properties, but at the same time they show low homogeneity. On the other hand T4 fibers show higher homogeneity, which is extremely important for further processing purposes; but they also possess a length 3 to 5 times lower than usual.

4.4 CNCs synthesis

As for CNFs synthesis, CNCs were not obtained from all the solid samples. T1 sample managed to eliminate only a small part of the amorphous domains in the cellulose structure, leading to mixed agglomerates whose size were of the order of magnitude of tens of micrometers. This happened mainly because the cellulose particles, even if ground, weren't sufficiently small for the hydrolysis step to be effective.
The characterization techniques comprise the measurement of crystallinity degree with DRX analysis, as well as viscosity and the related degree of polymerization.

Looking at Table 4.8 it is possible to see that T4 CNCs are able to reach extremely high levels of crystallinity compared to standard [13]; once more, this is allowed by the small dimensions of the solid particles, which are easier to be hydrolyzed.

Considering the degree of polymerization, the values for the three treatments are reported in Table 4.9, where it is seen that T4 CNCs were those with the highest value of DP. This is unexpected, because DP is substantially correlated to CNC's length, and - according to the previous results - a lower value

Table 4.8: CNCs' crystallinity degree.

TREATMENT	CRYSTALLINITY (%)
T2	49.91 ± 3.86
T3	69.73 ± 0.97
T4	91.20 ± 1.43

should have been obtained. But in fact it is possible to explain this anomalous value with the theory of Level-Off Degree of Polimerization (LODP) [42]: CNCs are produced through hydrolysis of the amorphous domains and actually, it is possible to reach complete dissolution of the amorphous regions; this level of crystallinity goes with a minimum of the DP, which is exactly the LODP. Since crystallinity index value for T4 CNCs is very high, it is possible that the sample had reached such level. Normally, it lies between $150 \div 400$ [14, 43] and in this case it would be expected to be smaller than the values for T2 and T3. A possible explanation is that LODP-CNCs tend to interact with each other and to form well ordered structures which might strongly affect the analysis of viscosity, thus affecting the final DP value.

Table 4.9: Intrinsic viscosity and DP measurements for CNCs.

TREATMENT	$[\eta]$ (mL/g)	DP
T2	72 ± 7	170 ± 17
T3	78 ± 33	185 ± 77
T4	115 ± 10	274 ± 24

Concerning the yield of CNCs' synthesis, the values are slightly more encouraging than those for CNFs, since all yields lie close to 50% of initial solid, as shown in Table 4.10.

Also for CNCs, an AFM analysis has been performed, whose results are shown in Figure 4.5. The same considerations previously carried out for CNFs hold in this case, since it is seen that: going further with treatments, the length decreases, the number of nanoscopic particle increases and the homogeneity increases. Contrarily to what stated for T4 CNFs, T4 CNCs show to be perfectly in line with literature values for length (reported in Table 4.11, along with width and aspect ratio as well), which usually span

Table 4.10: CNCs production yields.

TREATMENT	YIELD (% w/w)
T2	45.70 ± 2.64
T3	51.32 ± 3.23
T4	56.75 ± 1.38

between $70 \div 1000$ nm [13].

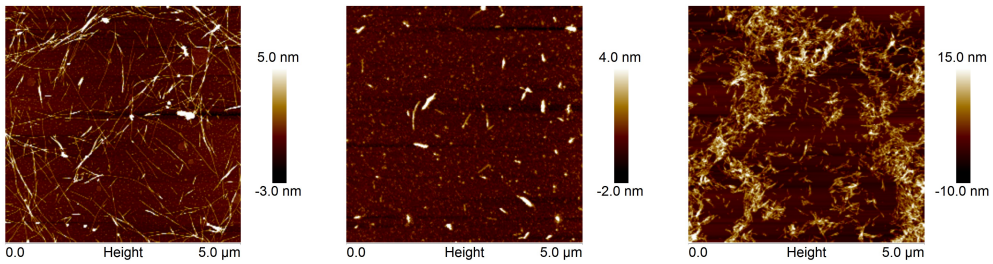

(a) T2 (b) T3 (c) T4

Figure 4.5: AFM images of CNCs 0.01% w/w aqueous solution.

Table 4.11: Length, thickness and aspect ratio for CNFs.

TREATMENT	LENGTH (nm)	WIDTH (nm)	ASPECT RATIO (l/w)
T2	1030 ± 625	3 ± 1	~ 208
T3	320 ± 85	5 ± 4	~ 64
T4	170 ± 60	7 ± 2	~ 24

To confirm the reported data about average particle size of the CNCs, a photo showing three samples for each treatment stage (in order from no.1 of T1 to no.12 of T4) is reported in Figure 4.6: it is possible to observe how cellulose fibrils progressively diminish their size down to the point that particles become almost invisible to human sight. As seen before, this goes with a narrower particle size distribution.

Figure 4.6: CNCs' samples: [1-2-3] from T1 (not proper CNCs), [4-5-6] from T2, [7-8-9] from T3 and [10-11-12] from T4.

4.5 Wastewater digestion

In parallel with nanocellulose production, liquid residue from the four treatments has been employed to feed different anaerobic reactors. The aim of this part of the work was to evaluate which one of the liquids was endowed with the highest biogas volumetric production; this will eventually help to portrait a more precise outline of the different output scenarios, thus allowing to choose the most appropriate treatment path.
After initial fill with available synthetically-fed sludge, reactors have been fed with properly diluted liquor from the initial treatment stage, following the schedule reported in Table 4.12: nutrients' concentration has been progressively raised through the cycles, in order to get bacteria accustomed to new feeding regime. Unluckily, further raise of fed COD hasn't been possible because of pH related issues; as a matter of fact, T3 and T4 feedings were characterized by extremely basic pH ($12 \div 14$) so that each time reactors were fed it was necessary to adjust internal pH in order to maintain best conditions for bacterial life (few drops of acid were sufficient to restore a pH level of $7 \div 7.5$). Note that chloridric acid has been employed, since it is the most compatible with the involved bacteria.

For each cycle of feeding, cumulated biogas production was daily measured

Table 4.12: COD[1] fed in reactors through the batch-cycles.

CYCLE	FED COD (g/L)			
	T1	T2	T3	T4
1	1.0	1.0	1.5	1.5
2	1.5	1.5	2.5	2.5
3	2.5	2.5	2.5	2.5
4	2.5	2.5	2.5	2.5
5	2.5	2.5	2.5	2.5

until it reached a constant value, meaning that nutrients' digestion would have stopped. Cumulative production throughout the different cycles is reported in Figure 4.7 (an exhaustive table with all values along with the graphics for each cycle may be found in Appendix A): it is possible to see how initial production is quite slow and relatively small (note that lower concentrations of nutrients were fed at the beginning) while increases in the last cycle.

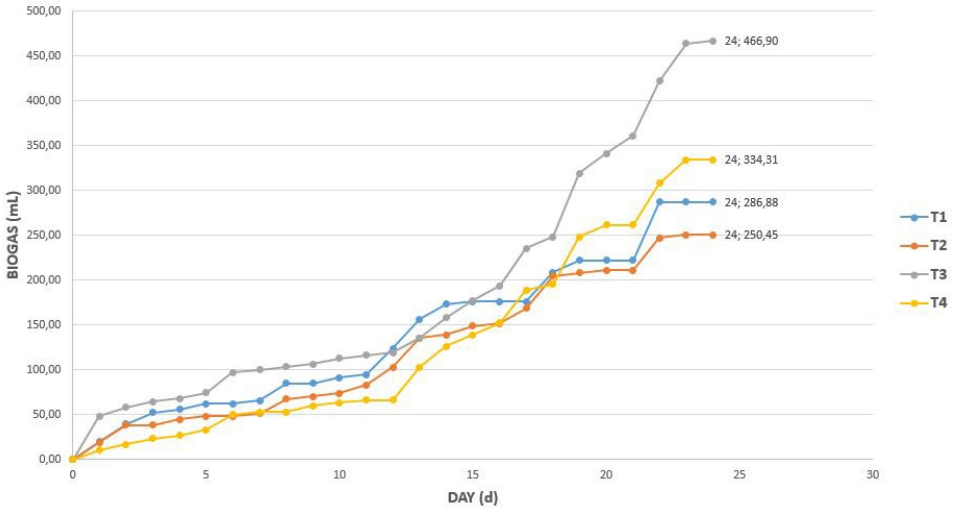

Figure 4.7: Cumulative biogas production for the different treatments.

[1]It is worth noting that reported values for COD correspond to reactors' internal concentration of nutrients which practically is the batch equivalent for organic loading rate (OLR). The expression "COD" might have be not been properly used in this context, nevertheless for practicality's purposes it has been hereafter employed anyhow.

Observing the different profiles for each treatment, it is evident that T3 and T4 liquids possess the highest potentials of biogas production, with T3 characterized by the highest one. Justifications to this result can be traced back to the fact that soda helped hydrolysis of nutrients, which were made available in less complex structures (e.g. simple monomers instead of macromolecules); this obviously enhances final biodegradability level of nutrients. Following this reasoning T4 liquid should be the one endowed with the highest biogas productivity, but actually T3 exceeded it by far. This might be explained with the high level of sodium which characterize T4 liquid: as a matter of fact it is proven that excessive concentrations of sodium are responsible for bacterial inhibition, therefore digestive actions worsens and leads to a lower biogas production [70].

Since T3 and T4 liquids gave the most encouraging results, their normalised productions have been calculated: as it is possible to see in Figure 4.8(a) and Figure 4.8(b), mass-normalized biogas production underwent a strong decrease when COD was raised, which was then recovered though. Averaged values for biogas production per kilogram of COD are reported in Table 4.13 along with methane yields, which were obtained multiplying normalized biogas production by methane fraction and dividing by the number of the days of the cycle. Actually, biogas experimental composition wasn't possible to calculate because of two reasons: firstly because the batch reactors employed were to be opened each time feeding was operated, thus letting a small amount of air entering in them and compromising any eventual measurement; secondly because it was impossible for the analyser to assess the composition of such a low flowrate. Therefore literature values have been taken as a reference: methane concentration of biogas coming from anaerobic digestion usually falls between $50 \div 75$ % of total flowrate and the upper limit value was taken as a good approximation of given conditions (mainly because measurements were taken in batch, which gives the digestion longer time to consume previously produced CO_2 in order to synthesize more CH_4) [84].

The mentioned values stand slightly below than common lower limit for similar effluents (e.g. pulp and paper mill wastewater sludge), which lies around 200 L_{BIOGAS}/kg_{COD} [85]. In fact, much higher values might be reached (up to 1000 L_{BIOGAS}/kg_{COD} [86]), but - since reactors had a batch structure and couldn't be loaded with high values of COD - results are quite satisfying after all.

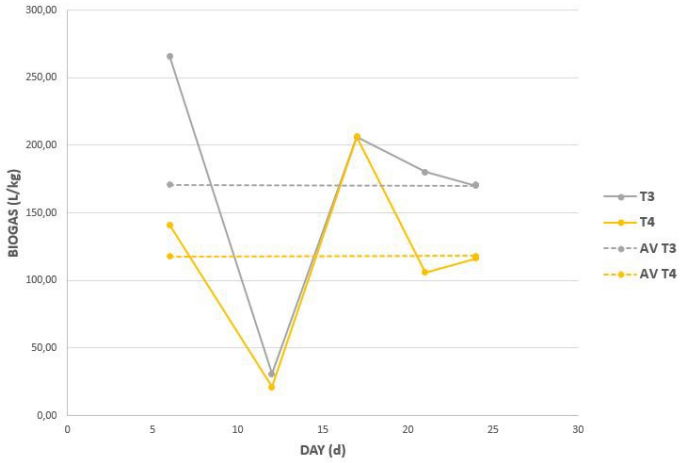

(a) Normalized biogas production.

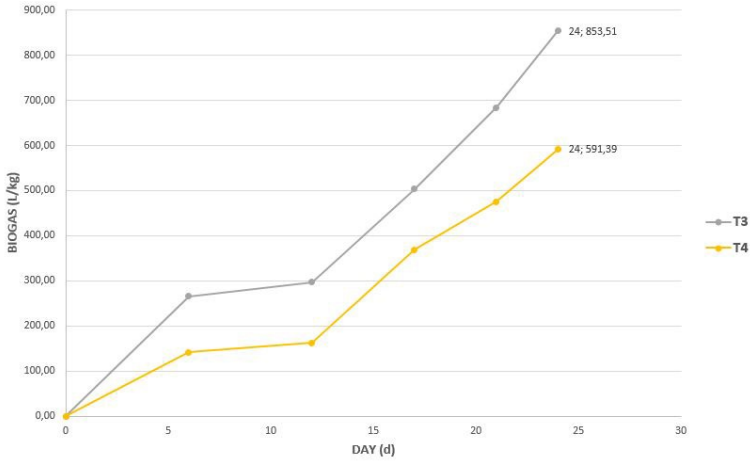

(b) Cumulated production

Figure 4.8: Average and cumulated normalized biogas production.

Table 4.13: Average biogas production potentials.

TREATMENT	AV. BIOGAS PRODUCTION (L_{BIOGAS}/kg_{COD})	AV. METHANE YIELD ($L_{METHANE}/kg_{COD}d$)
T3	170.70	38.68
T4	118.28	26.60

Chapter 5

Simulation

In this chapter, the results collected from laboratory were employed to design and simulate the operation of a waste treatment plant. Particular relevance has been given to the construction of a simple, Matlab-based model for anaerobic digestion, which has been employed to fit experimental data of biogas production.

5.1 Treatment pathway choice

First of all, it has been necessary to choose the best possible scenario from those investigated, whose results would have been the starting base for the development of the simulation. T1 and T2 cases have been excluded for the low quality of the outputs, along with the impossibility of synthesizing some of them. As far as T3 and T4 are regarded, both of them have shown to produce mostly satisfying results:

- ***T3*** demonstrated to produce nanocellulose characterized by much higher aspect ratio than T4 and moreover had the highest biogas production potential;
- ***T4*** led to produce super-high quality CNCs and CNFs - though mostly shorter than average - which showed high homogeneity.

Another important parameter which has been considered is the solid yield of the treatments, which favoured T3.
Nevertheless the final choice leaned towards T4, mainly because of the elevated quality of nanocellulose output, which outdid T3's by far; besides, as nanocellulose production is a highly investigated topic in the last years,

high quality CNCs and CNFs are the standard for nowadays market.

5.2 Process design

5.2.1 Waste streams

Literature data related to breweries' BSG and wastewater production have been analyzed in order to determine all the values to be employed as a starting point for process simulation.

First of all, yearly average beer production has been assessed: values may strongly vary depending on the size of the plant, starting from 1000 hL/y for a new-born micro-brewery, to $50 \cdot 10^3$ hL/y for a small hand-crafted production until millions of hectoliters per year for world's largest plants [87].
As far as BSG is regarded, its production is related to the very value of beer and it is usually agreed upon 20 kg_{BSG}/hL_{BEER} [88, 89], measure that refers to wet BSG. As a matter of fact, freshly produced BSG is usually characterized by a humidity percentage of 75 %, that leads to a a value of 5 kg_{BSG}/hL_{BEER} of dry BSG production.
Lastly, it is necessary to talk about wastewater production, which is related to beer production as well: common values for water consumption range between $4 \div 11$ hL_{WATER}/hL_{BEER} [87] depending on the internal water management efficiency of the plant. Moreover, it has to be pointed out that the wastewater stream possesses a certain value of COD itself, since it derives from several barley washings along with its steeping phase before fermentation; once again, the value of this parameter may strongly vary, spanning between $800 \div 5000$ mg/L (with some peaks of 10000 mg/L) [90]

Since the brewery that supplied the BSG for this study was an average plant producing hand-crafted beer, its production have been chosen accordingly. For what regards the other values related to wastewater production and its COD, average values have been selected and are shown[1] in Table 5.1.

[1]Note that for the sake of a clearer study, starting value of BSG daily production has been rounded to the one reported and used to obtain the other values.

Table 5.1: Waste production and specifics.

BEER PRODUCTION (hL_{BEER}/y)	53250
WET-BSG PRODUCTION (ton/d)[2]	3
DRY-BSG PRODUCTION (ton/d)	0.75
WATER CONSUMPTION (hL_{WATER}/hL_{BEER})	7.5
WAST-WAT PRODUCTION (m^3/d)	97.5
$COD_{WAST\text{-}WAT}$ (kg/m^3)	3

5.2.2 Process structure

The design of the process structure has been realized considering both of the two possible pathways for solid processing, that is to say production of CNFs and CNCs. The obtained organization is reported in Figure 5.1 and shows all the main passages for liquid and solid treatment.
Reviewing each passage it must be noted that:

- ***the stream of wastewater*** coming directly from the brewery is employed both to *a)* further dilute wet-BSG up until the concentration provided by its treatment protocol and *b)* dissolve the necessary amount of soda to be added to the BSG;
- ***the treatment box*** includes all the explained passages of T4 (grinding, boiling, soda, autoclave);
- ***first centrifugation passage*** completely separates liquid and solid parts (though obtained solid is supposed to set to dry next, for simplicity's sake during the following passages water coming directly from the treatment is assumed to wholly move to the digester, without losses due to humidity of the solid);
- ***the anaerobic digester*** will produce a stream of partially cleaned water and digestate, which in this design is supposed to need further treatment (e.g. a passage in a second digester, most preferably an aerobic one);
- ***CNFs and CNCs*** production sections are designed to assess the amount of final product considering the processing of 100 % of available solid each (i.e. the amount of solid coming directly from first centrifugation is employed - as it is - both for CNFs and CNCs), in order to evaluate full production potential per type of product.

[2]To convert from yearly values to daily ones an approximated number of operation days per year has been set to 355 d.

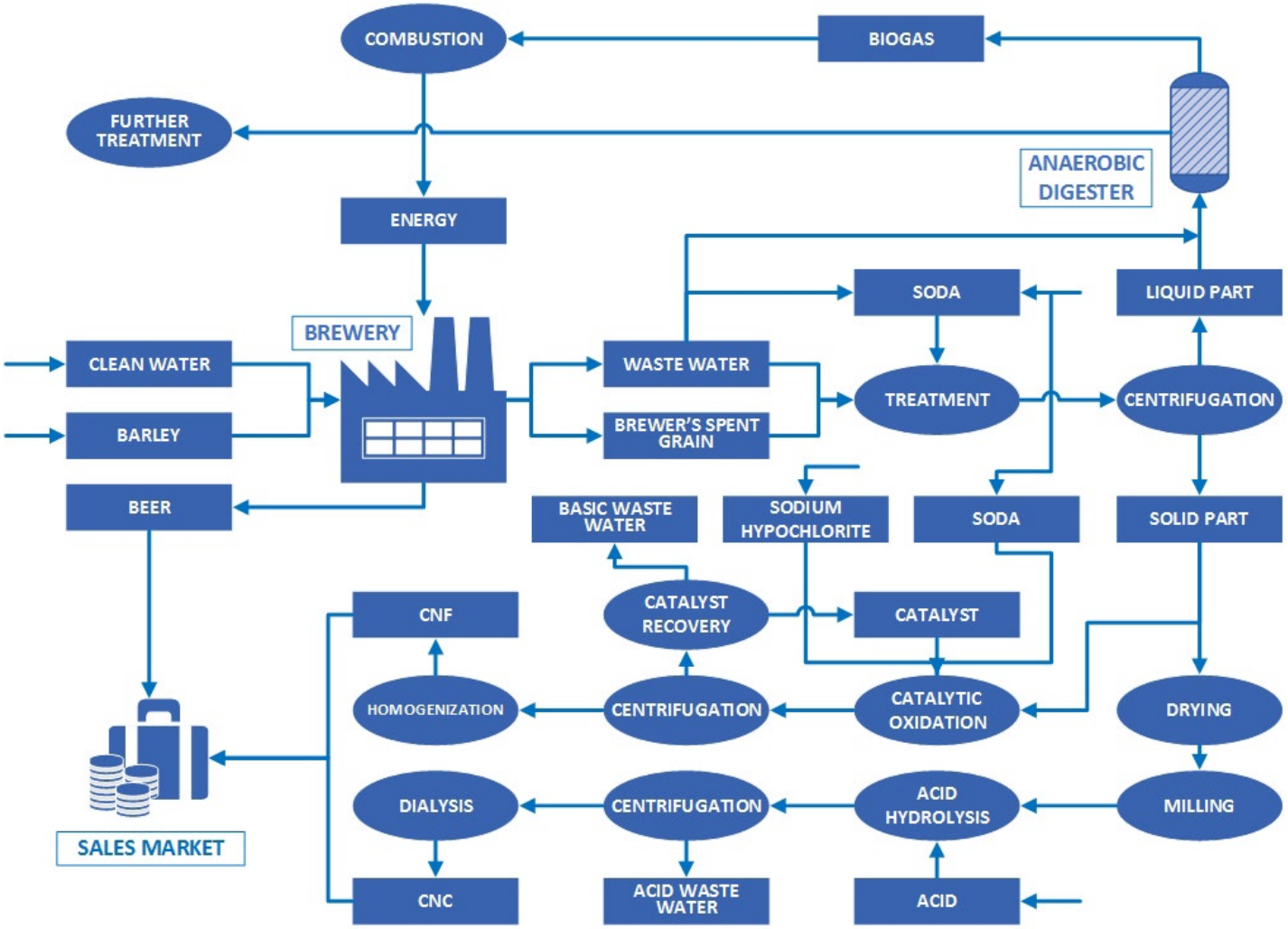

Figure 5.1: Design of the process for waste treatment.

5.3 Digester modeling

After designing the overall process, it has been necessary to develop a computer-based model to allow the calculation of the output stream related to the anaerobic digester; Matlab routines have been developed to simulate both batch and CSTR behaviors of anaerobic digestion, the former employed to fit experimental data, the latter to actually calculate the final output of the digester in the designed conditions.

5.3.1 Batch model

Batch-structured routine has been employed to fit data coming from cycle 5 T4 biogas production (see Appendix A). It was implemented inside of the model employing an iterative routine which calculated consumption-production rates based on concentrations at $(N)^{th}$ step and employing them to update $(N+1)^{th}$ concentrations with a time step of 0.01 h.
The kinetic model comprehends 19 different parameters, whose literature values have been taken as a starting point for fitting. In order to perform it, it has been necessary to choose which were the most influent parameters to modify and which were those to be fixed: first attempts with this approach were all unsuccessful and led to poor quality results, no matter how many parameters were set free. This happened mainly because even slight variations[3] of many parameters produced significative changes in the curve shape and location.
Therefore a different approach has been employed, characterized by two consecutive step:

- ***step I:*** a preliminary modification of the literature value of the parameters' set, which has been realized with the help of an annealing algorithm. Strong variations in the output of a parameter characterized those which were to be set free for final fitting;
- ***step II:*** proper fitting with minimization of quadratic error, employing *a)* initial literature data for parameters which didn't show any variation during annealing, *b)* annealing-modified values for parameters that showed slight variations during annealing and *c)* setting free those parameters which strongly varied during annealing.

[3]Note that the mentioned "variations" refer to tiny adjustments to the value, which fell inside of the literature range by far.

Annealing algorithm allowed for recognition of the critical parameters (such values strongly diverged from literature ones) which were found to be the hydrolysis constants for proteins and cellulose; these two parameters were then coupled with one more - maximum specific growth rate for methanogenic bacteria - towards the variation of which, the fitting proved to be very sensible to. Fitting was eventually performed employing these three parameters and fixing all the remaining others.

Boundary conditions for the simulation were derived from the experimental values: nutrients' concentration was set according to cycle feeding (see Table 4.12) and its distribution was obtained by difference observing solid composition before and after T4 (composition percentages are reported in Appendix A); moreover, bacterial concentration was derived from the TSS (Total Suspended Solids) of the reactor - the sludge of which - has been collected in order to be used in this study.

Final values of all the parameters are shown in Table 5.2 and it is important to remark the unusual output obtained for the two hydrolysis constants for proteins and cellulose. A possible explanation for such strong variations might be derived from the assumed composition entering the reactor: as a matter of fact, nutrients distribution has been obtained by difference (calculating the dissolved part of the treated solid), but in fact the strong concentration of soda employed for T4 almost certainly affected nutrients' structure. Indeed, proteins may easily have been degraded by soda, leading to an extremely low concentration of actual proteins (and, of course, an unexpected concentration of other molecules, mostly undigestible for bacterial populations). Therefore the hydrolysis constant for proteins resulted to be very low (two degrees of magnitude lower than average), because actually proper protein structures might be practically absent.
A similar explanation holds for cellulose, which was probably hydrolyzed to glucose by soda; further degradation isn't likely because of aromatic ring's strength, therefore a high concentration of glucose might have entered the system from the beginning (while model expected to have only cellulose). This led to a high value of cellulose hydrolysis constant in order to compensate for the partial hydrolysis that already took place outside the reactor.

Generated curve for methane batch production is reported in Figure 5.2: it is evident that the fitting of the experimental points has achieved a high level of precision, with a coefficient of determination $R^2 = 99.82$ % and an adjusted coefficient $R^2_{ADJ} = 99.73$ %. Simulated profiles for CH_4 - CO_2 -

Table 5.2: Values of the parameters through fitting steps ("UNCH" mark means that the value hasn't changed from the previous step, while final values are framed).

PARAMETER	LITERATURE VALUE	ANNEALING VALUE	FITTING VALUE
	HYDROLYSIS CONSTANTS (1/h)		
$k_{h,LIGN}$ [91]	0.00173	0.00345	$UNCH$
$k_{h,PROT}$ [92]	0.03125	0.00089	0.00014
$k_{h,FAT}$ [92]	0.03400	0.02384	$UNCH$
$k_{h,CELL}$ [53]	0.07088	0.76251	0.46038
	MAXIMUM SPECIFIC GROWTH RATES (1/h)		
$\mu_{max,ACID}$ [53]	0.30000	$UNCH$	$UNCH$
$\mu_{max,ACET}$ [53]	0.01725	0.01454	$UNCH$
$\mu_{max,METH}$ [53]	0.00149	0.00123	0.00108
	DECAY RATES (1/h)		
b_{ACID} [54]	0.00208	$UNCH$	$UNCH$
b_{ACET} [54]	0.00208	$UNCH$	$UNCH$
b_{METH} [54]	0.00041	$UNCH$	$UNCH$
	SEMI-SATURATION CONSTANTS (g/L)		
$k_{s,ACID}$ [53]	0.42700	0.58302	$UNCH$
$k_{s,ACET}$ [53]	0.16600	0.15276	$UNCH$
$k_{s,METH}$ [53]	0.16500	0.12833	$UNCH$
	BIOMASS YIELD FACTOR ($g_{biomass}/g_{substrate}$)		
$Y_{X_{ACID}/GLUC}$ [54]	0.15000	0.17221	$UNCH$
$Y_{X_{ACID}/AMIN}$ [53]	0.20500	0.18161	$UNCH$
$Y_{X_{ACET}/VALE}$ [78]	0.05000	$UNCH$	$UNCH$
$Y_{X_{ACET}/BUTY}$ [53]	0.05800	$UNCH$	$UNCH$
$Y_{X_{ACET}/PROP}$ [53]	0.03700	$UNCH$	$UNCH$
$Y_{X_{ACET}/PHEN}$ [53]	0.10000	0.10945	$UNCH$
$Y_{X_{ACET}/LCFA}$ [53]	0.11000	$UNCH$	$UNCH$
$Y_{X_{METH}/ACET}$ [53]	0.04100	$UNCH$	$UNCH$
$Y_{X_{METH}/H2}$ [53]	0.04500	$UNCH$	$UNCH$

H_2 and for dissolved components are reported in Appendix A.

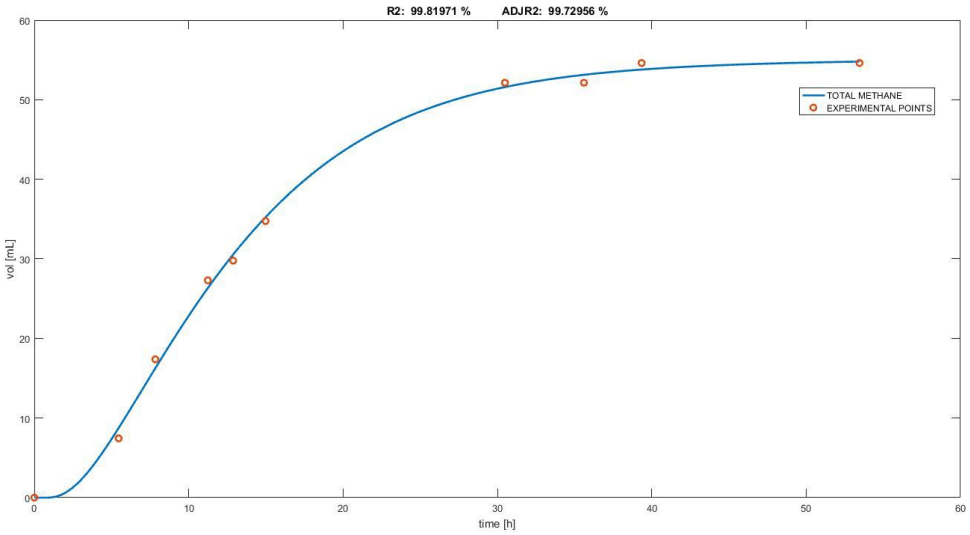

Figure 5.2: Fitting of cycle 5 batch methane production.

It has to be pointed out that in order to ensure better fitting performance, experimental points for methane production have been shifted by 10 % of the total time-scale of the cycle: this delay is consistent with the fact the the model starts "from zero" (i.e. with initial null value for monomers, fatty acids, carbon dioxide and hydrogen), while real reactor - even if in low concentration - was provided with some nutrients from the previous feeding cycle. As a consequence real biogas production can start almost immediately, while the simulated one shows a delay, which has been properly taken into account in this way.

5.3.2 CSTR model

While perfect for experimental data fitting, the batch routine developed in the previous step is useless for operative design of the treatment plant: as a matter of fact, the process is meant to be working in continuous and therefore it has been required to develop a second routine, following a CSTR balance.

In order to define the employed balance, some assumptions have to be carried out first:

- ***the liquid flowrate*** entering the reactor has been set equal to the one coming out from it in terms of volume;
- ***COD components*** and all the intermediates produced during digestion (i.e. lignin, proteins, fats, cellulose, their hydrolyzed monomers and fatty acids) were assumed to be fully dissolved inside the liquid and to never precipitate. In this way outlet value of COD has to take into account their concentration;
- ***biogas components*** were supposed to have null concentration in the liquid, so that it was not balanced referring their amount to the flowrate. This means that gasses only had a production term referred to the kinetics and a massive outlet representing the gaseous flowrate exiting the reactor;
- ***bacteria's concentration*** inside of the reactor has been assumed constant, as the bacterial growth is counterbalanced by digestate outlet, which hasn't been accounted in this model.

Therefore two different balances have been employed, one for the dissolved components:

$$\dot{V}(\Delta C_i) = r_i V_R \tag{5.1}$$

Where $\dot{V}$ is the volumetric flowrate entering and exiting the reactor expressed in $[m^3/d]$, ΔC_i is the difference between inlet and outlet concentration of the i-component expressed in $[kg/m^3]$, r_i is the production term of the i-component due to digestion kinetics expressed in $[kg/m^3 d]$ and V_R is the volume of the reactor expressed in $[m^3]$.
Contrary for biogas components the following balance has been employed:

$$\dot{M}_i^{OUT} = r_i V_R \tag{5.2}$$

Where $\dot{M}_i^{OUT}$ is the massive outlet term, representing the gaseous flowrate coming out from the reactor.

Applying these balances to the digestion model, the profiles shown in Figure 5.3 have been obtained: inlet flowrate and COD have been derived from previously chosen waste production and the volume of the reactor has been

iteratively changed in order to obtain the reported plots.
It is easy to note that for high OLR methane production sharply decreases (the reactor isn't able to deal with such a great amount of nutrients, especially because of lignin, which hydrolyzes with extremely low rates). At the same time it is possible to see that excessively increasing the volume of the reactor (i.e. high values of HRT) is completely useless, given that the increase in methane production is very small.
As a matter of fact, plotting methane production divided by reactor volume over HRT, highlights the presence of an optimum value of HRT (thus reactor volume), as it is shown in Figure 5.4: at a value of $\sim$ 7.5 d, specific methane production is maximized and - employing this value - Table 5.3 reports operation specifics for the CSTR-digester.

Table 5.3: Optimized operation values for the digester in CSTR conditions.

INLET COD (kg/m^3)	7.45
INLET FLOW (m^3/d)	99.75
REACTOR VOLUME (m^3)	752.06
HRT (d)	7.54
OLR (kg/m^3d)	0.99
COD REMOVAL (%)	59.43
TOTAL METHANE PRODUCTION (m^3/d)	36.05
V_R-NORMALIZED METHANE PRODUCTION (L/m^3d)	0.048
METHANE YIELD ($L/kg_{COD}d$)	81.64

Comparing the methane yield here calculated with the value obtained from experimental batch reactor (i.e. 26.60 $L/kg_{COD}d$), it is possible to see how methane yield shows a higher value after the simulated CSTR optimization (three times higher). This happens because bacterial growth is kept at its maximum thanks to appropriate design of the process.

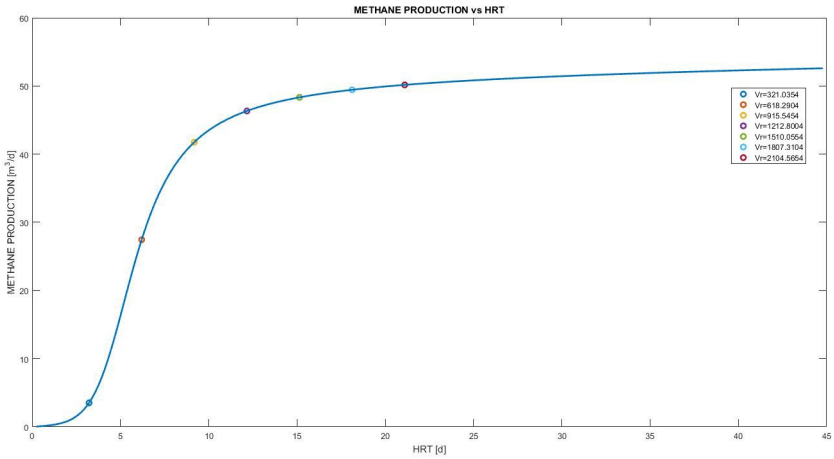

(a) Methane vs HRT

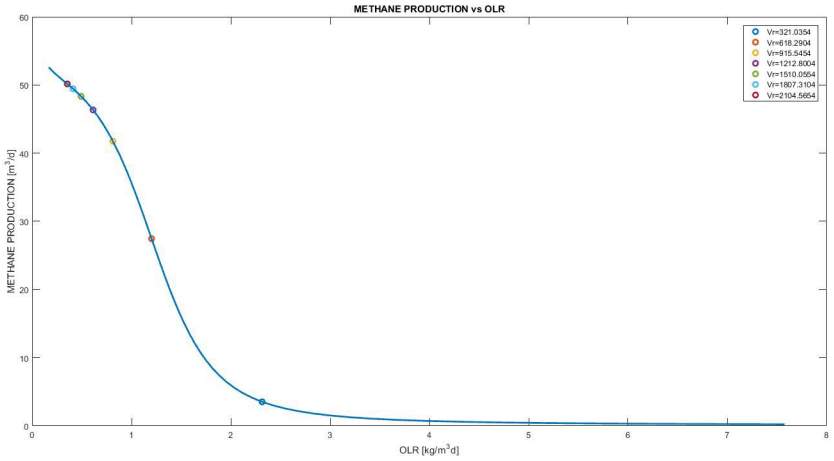

(b) Methane vs OLR

Figure 5.3: Plots for methane production vs (a) HRT and (b) OLR.

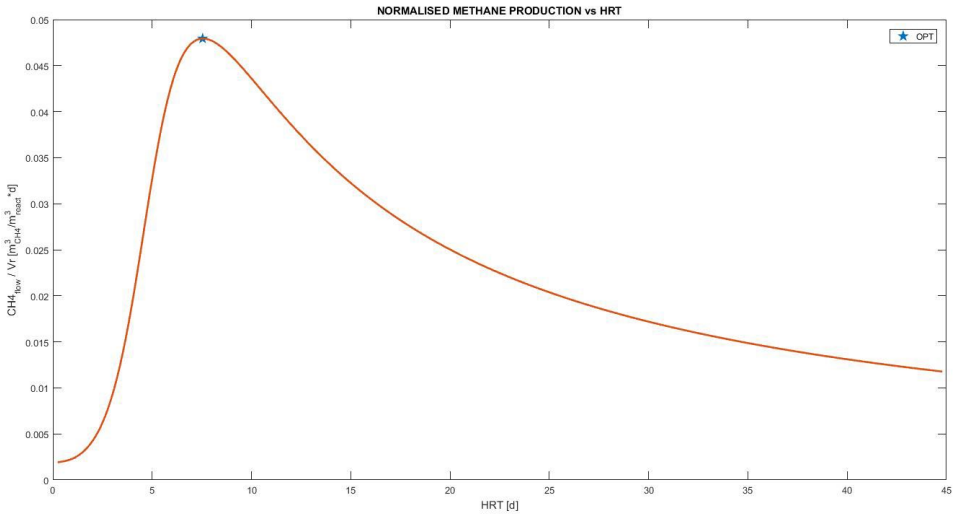

Figure 5.4: Reactor-volume-normalized methane production over HRT.

5.4 Process performances

In order to summarize the so-far-obtained results, three tables are proposed hereafter, which are related to initial wastes, CNFs - CNCs production[4] and digester's outlet (respectively Tables 5.4, 5.5, 5.6).
It is interesting to note that final value of COD after anaerobic treatment equals the initial one: this happens because the removed COD perfectly matches BSG treatment's liquor contribution. Therefore, further treatments for digester's outlet stream are mandatory. But on the other hand, designed digestion allows for a significative methane production, which may be employed as a source of energy.
Nanocellulose production give small fractions of final product (compared to initial amount of solid waste), nevertheless their commercial values is quite high though, compensating for their low yield.

[4]Remember that values are reported as if all the available solid was to entirely be used per each one of the products.

Table 5.4: Wastes inlet.

WASTEWATER (m^3/d)	97.5
COD (kg/m^3)	3
WET-BSG (ton/d)	3
DRY-BSG (ton/d)	0.75

Table 5.5: CNFs - CNCs production.

CNFs (kg/d)	38.25
CNCs (kg/d)	64.14

Table 5.6: Digestor's outlet.

WASTEWATER (m^3/d)	99.75
COD (kg/m^3)	3
METHANE (m^3/d)	36.05

5.5 Future developments

As first and most important possible future improvement, pilot-plant reactors for anaerobic digestion may be set up, in order to allow for a continuous configuration, along with a better control of the key parameters for the process (pH, temperature, OLR, etc.).
Further studies may focus on the identification of alternative preliminary treatment paths for BSG, in order to assess optimum conditions. In particular, sodium chloride's effect on BSG particles' final size should be evaluated, as to maximize nanocellulose aspect ratio without compromising other quality parameters (crystallinity degree, transmittance and centrifugal yield, etc.). Since sodium chloride probably effected anaerobic digestion as well, its effect may be investigated on that too.
Other favourable improvements may be provided to the structure of the model, in order to account for inhibition and other physicochemical reactions such as dissolution, absorption, coalescence, precipitation, etc. Moreover, acid and basic waters from nanocellulose synthesis steps, may be included inside of the process loop: they might be reused in pH control of the digester and initial BSG treatment as well.

Lastly, economic analysis may be performed on the obtained results, to help assessing the feasibility of the process as a real option for breweries.

Chapter 6

Conclusions

This work evidenced the actual viability of the proposed waste treatment process. Satisfactory results were obtained for what regards both nanocellulose and biogas production.
CNFs showed to reach extremely high homogeneity (i.e. 100 % centrifugal yield was obtained) but average particle length was lower than standard. CNCs scored perfect values both for crystallinity degree and particle size, proving to be the most interesting pathway for solid treatment, so far.
Concerning wastewater treatment, methane yield was about half common lower limit for similar applications, but it is worth noting that the experimental apparatus for anaerobic digestion was extremely simple.
In conclusion, the promising results obtained suggest that feasibility studies in this field are desirable to be performed in breweries.

Appendices

Appendix A

Results

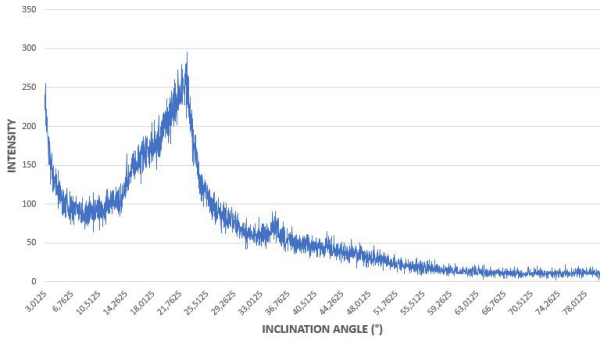

(a) Untreated BSG

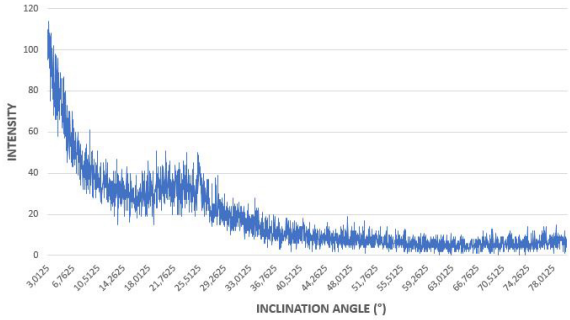

(b) BSG ashes

Figure A.1: Comparison between unstreated BSG (a) and BSG ashes (b) with DRX analysis: the peak associated to cellulose (around 22°) is extremely disturbed for the presence of silicates in BSG, which remains in the ashes after incineration at 575 ° C.

Table A.1: Treated BSG composition.

TREATMENT	LIGNIN (% w/w)	PROTEINS (% w/w)	FATTY ACIDS (% w/w)	CELLULOSE (% w/w)	ASHES (% w/w)
T1	15.16 ± 0.08	22.49 ± 2.61	19.88 ± 1.13	38.67 ± 3.83	3.80 ± 0.01
T2	16.05 ± 0.24	23.05 ± 0.50	12.26 ± 0.26	44.46 ± 1.66	4.18 ± 0.66
T3	11.83 ± 0.11	12.32 ± 0.18	5.88 ± 0.45	59.98 ± 1.18	9.99 ± 0.44
T4	6.46 ± 0.13	1.28 ± 0.03	2.95 ± 0.06	76.50 ± 1.37	12.81 ± 1.15

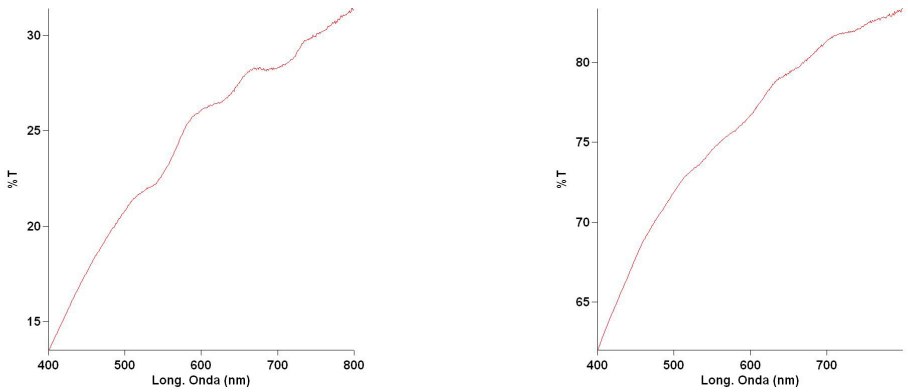

(a) T3 CNFs

(b) T4 CNFs

Figure A.2: Plots for T3 (a) and T4 (b) transmittance sweep between 400 and 800 nm.

Table A.2: Cumulative biogas production (BP) through the five cycles of batch-feeding.

DAY	T1-BP (mL)	T2-BP (mL)	T3-BP (mL)	T4-BP (mL)
0	0.00	0.00	0.00	0.00
1	19.56	19.20	48.30	9.93
2	39.12	38.40	57.96	16.55
3	52.16	38.40	64.40	23.17
4	55.42	44.80	67.62	26.48
5	61.94	48.00	74.06	33.10
6	61.94	48.00	96.60	49.65
7	65.20	51.20	99.82	52.96
8	84.76	67.20	103.04	52.96
9	84.76	70.40	106.26	59.58
10	91.28	73.60	112.70	62.89
11	94.54	83.20	115.92	66.20
12	123.88	102.40	119.14	66.20
13	156.48	135.30	135.24	102.61
14	172.78	138.59	157.78	125.78
15	176.04	148.46	177.10	139.02
16	176.04	151.75	193.20	152.26
17	176.04	168.20	235.06	188.67
18	208.64	204.39	247.94	195.29
19	221.68	207.68	318.78	248.25
20	221.68	210.97	341.32	261.49
21	221.68	210.97	360.64	261.49
22	286.88	247.16	321.82	307.83
23	286.88	250.45	463.68	334.31
24	186.88	250.45	466.90	334.31

Table A.3: Composition of liquid entering the anaerobic digester.

NUTRIENT	CONTENT (% w/w)
Lignin	23.92
Proteins	26.16
Fatty acids	23.00
Cellulose	24.90

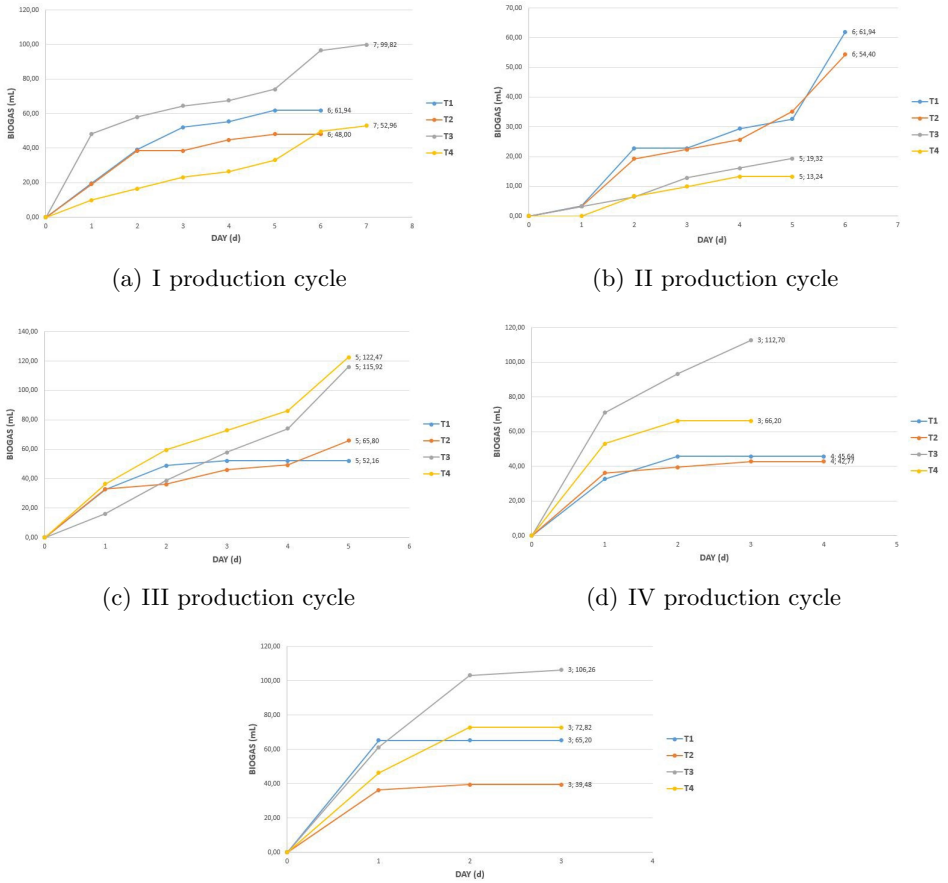

(a) I production cycle

(b) II production cycle

(c) III production cycle

(d) IV production cycle

(e) V production cycle

Figure A.3: Plots for cumulative biogas production during the five cycles of batch-feeding.

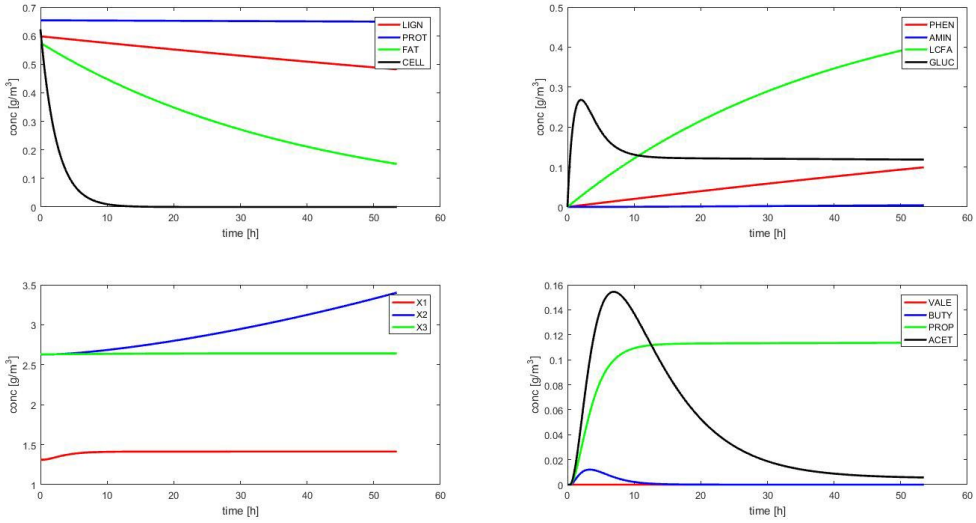

Figure A.4: Batch digestion simulated profiles for: macronutrients (upper-left), hydrolyzed monomers (upper-right), bacteria populations (lower-left) and volatile fatty acids (lower-right).

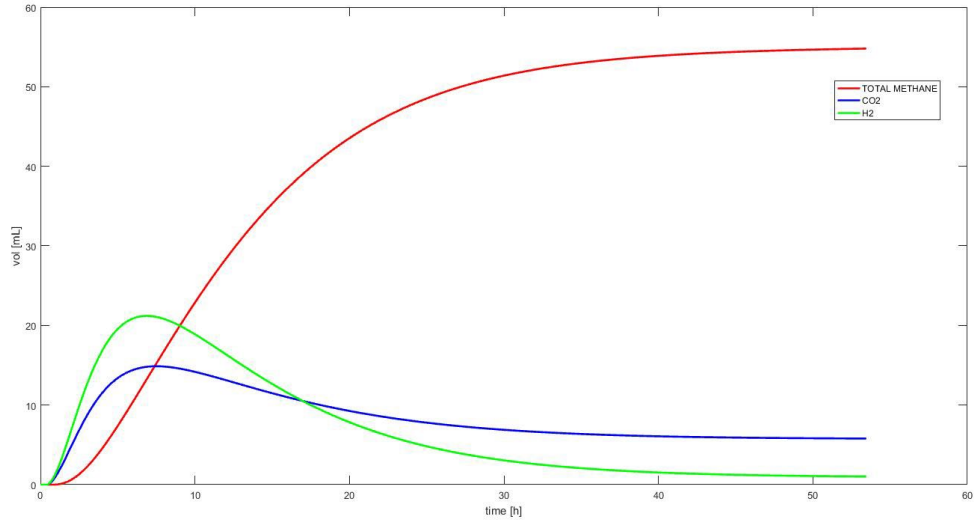

Figure A.5: Batch digestion simulated profiles for CH_4 - CO_2 - H_2.

Bibliography

[1] Schildbach R., Ritter W., Schmithals K., Burbidge M. (1992) "*New developments in the environmentally safe disposal of spent grains and waste kieselguhr from breweries*" Proceedings of the convention-institute of brewing (Asia Pacific Section), Vol. 22: 139-143.

[2] Aikat K., Bhattacharyya B.C. (2000) "*Optimization of some parameters of solid state fermentation of wheat bran for protease production by a local strain of rhizopus oryzae*" Acta biotechnologica 20: 149-159.

[3] Mussatto S.I., Roberto I.C. (2004) "*Alternatives for detoxification of diluteacid lignocellulosic hydrolyzates for use in fermentative processes: a review.*" Bioresource technology 93: 1-10.

[4] Kabel M.A., Carvalheiro F., Garrote G., Avgerinos E., Koukios E., Parajo J.C., Girio F.M., Schols H.A., Voragen A.G.J. (2002) "*Hydrothermally treated xylan rich byproducts yield different classes of xylo-oligosaccharides*" Carbohydrate polymers 50: 47-56.

[5] Bartolome B., Gomez-Cordoves C. (1999) "*Barley spent grain: release of hydroxycinnamic acids (ferulic and p-coumaric acids) by commercial enzyme preparations*" Journal of the science of food and agriculture 79: 435-439.

[6] Mussatto S.I., Roberto I.C. (2002) "*Xylitol: an edulcorant with benefits for human health*" Brazilian journal of pharmaceutical sciences 38: 401-413.

[7] Balea A., Merayo N, De La Fuente E., Negro C., Blanco A. (2016) "*Assessing the influence of refining, bleaching and TEMPO-mediated oxidation on the production of more sustainable cellulose nanofibers and their application as paper additives*" Industrial crops and products 97: 374-387.

[8] Iman Shahabi-Ghahafarrokhi et al. (2015) "*Preparation and characterization of nanocellulose from beer industrial residues using acid hydrolysis/ultrasound*" Biomacromolecules 9 (6): 529-536.

[9] D. Fengel, G. Wegener, "*Wood: chemistry, ultrastructure, reactions*" Walter de Gruyter (1984).

[10] *http://genomics.energy.gov* (Last access on 27/03/2017)

[11] A. Dufresne, "*Nanocellulose: from nature to high performance tailored materials*" Walter de Gruyter (2013).

[12] R.J. Moon, "*MaGraw-Hill Yearbook in science and technology*" McGraw-Hill (2008): 225-228.

[13] Johnsy G. et al. (2015) "*Cellulose Nanocrystals: synthesis, functional properties and applications*" Nanotechnologies, Science and Applications 2015-8: 45-54.

[14] Habibi Y. at al. (2010) "*Cellulose nanocrystals: chemistry, self-assembly and applications*" Chemical reviews 110 (6): 3479-3500.

[15] E. Sjostrom "*Wood Chemistry: Fundamentals and Applications*" 2nd ed., California, Academic Press Inc (1993).

[16] Lavoine N., Desloges I., Dufresne A., Bras J. (2012) "*Microfibrillated cellulose - its barrier properties and applications in cellulosic materials: a review*" Carbohydrate Polymers 90: 735-764.

[17] Lin N., Huang J., Dufresne A. (2012) "*Preparation, properties and application of polysaccharide nanocrystals in advanced functional nanomaterials: a review*" Nanoscale 4: 3274-3294.

[18] Azizi Samir A. S., Alloin F:, Dufresne A. (2005) "*Review of recent research into cellulosic whiskers, their properties and their application in nanocomposite field*" Biomacromolecules Vol. 6, No. 2: 612-626.

[19] J. Lemaitre, et al. "*Mecanique des materiaux*" 3rd ed., Dunod (2009).

[20] Yeh W.-Y., Young R. J. (1999) "*Molecular deformation processes in aromatic high modulus polymer fibres*" Polymers 40: 857-870.

[21] Dufresne A. (2013) "*Nanocellulose: a new ageless bionanomaterial*" Material today Vol. 16, No. 6: 220-227.

[22] Clowes F. A. L., Juniper B. E. "*Plant cells*" Blackwell scientific publications Ltd., Oxford (1968): 203-297.

[23] Alemdar A., Sain M. (2008) "*Isolation and characterization of nanofibers from agricultural residues - Wheat straw and soy hulls*" Bioresource technology 99: 1664-1671.

[24] Henriksson M., Berglund L. A., Isaksson P., Lindstrom T., Nishino T. (2008) "*Cellulose nanopaper structures of high toughness*" Biomacromolecules 9: 1579-1585.

[25] Shinoda R., Saito T., Okita Y., Isogai A. (2012) "*Relationship between length and degree of polymerization of TEMPO-oxidized cellulose nanofibrils*" Biomacromolecules 13: 842-849.

[26] Hietala M., Mathew A. P., Oksman K. (2013) "*Bionanocomposite of thermoplastic starch and cellulose nanofibers manufactured using twin-screw extrusion*" Europea polymer journal 49: 950-956.

[27] Turbak A. F. (1983) "*Newer cellulose solvent systems*" Wood and agricultural residues: 87-99.

[28] Abe K., Iwamoto S., Yano H. (2007) "*Obtaining cellulose nanofibers with a uniform width of 15 nm from wood*" Biomacromolecules 10: 3276-3278.

[29] Chakraborty A., Sain M., Kortschot M. (2005) "*Cellulose microfibrils: A novel method of preparation using high shear refining and cryocrushing*". Holzforschung 59(1): 102-107.

[30] Zhao et al. (2007) "*A green route to prepare cellulose acetate particle from ramie fiber*" Reactive and functional polymers 67 (2): 104-112.

[31] Herrick et al. (1983) "*Microfibrillated cellulose: morphology and accessibility*". Journal of applied polymer science, Applied polymers symposium 37(9): 797-813.

[32] Isogai A., Saito T., Fukuzumi H. (2011) "*TEMPO-oxidized cellulose nanofibers*". Nanoscale 3: 71-85.

[33] Walecka J.A. (1956) "*An investigation of low degree of substitution carboxymethylcelluloses*" Tappi 39: 458-463.

[34] Henrissat B. (1994) "*Cellulases and their interaction with cellulose*" Cellulose 1: 169-196.

[35] Liu H., Fu S.Y., Zhu J.Y., Li H., Zhan H.Y. (2009) "*Vizualization of enzymatic hydrolysis of cellulose using AFM phase imaging*" Enzyme Microbial Technology 45: 274-281.

[36] Newman R.H., Hemmingson J.A. (1995) "*Carbon-13 NMR distinction between categories of molecular order and disorder in cellulose*" Cellulose 2: 95-110.

[37] De Souza Lima M.M., Borsali R. (2004) "*Rod like cellulose microcrystals: structure, properties and applications*" Macromolecular Rapidid Communication 25: 771-787.

[38] Domingues R.M., Gomes M.E., Reis R.L. (2014) "*The potential of cellulose nanocrystals in tissue engineering strategies*" Biomacromolecules 15: 2327-2346.

[39] Beck-Candanedo S., Roman M., Gray D.G. (2005) "*Effect of reaction conditions on the properties and behavior of wood cellulose nanocrystal suspensions*" Biomacromolecules 6: 1048-1054.

[40] Araki J., Wada M., Kuga S. (2001) "*Steric stabilization of a cellulose microcrystal suspension by polyethylene-glycol-grafting*" Langmuir 17: 21-27.

[41] De Menezes A.J., Siqueira G., Curvelo A.A., Dufresne A. (2009) "*Extrusion and characterization of functionalized cellulose whiskers reinforced polyethylene nanocomposites*" Polymers 50: 4552-4563.

[42] Battista O. A. et al. (1956) "*Relation to polyphase cellulose structure of cellulose fibers*" Industrial and engineering chemistry 48 (2): 333-335.

[43] Hakansson H., Ahlgren P. (2005) "*Acid hydrolysis of some industrial pulps: effect of hydrolysis conditions and raw material*" Cellulose 12: 177-183.

[44] Iwamoto S., Kai W., Isogai A., Iwata T. (2009) "*Elastic modulus of single cellulose microfibrils from tunicate measured by atomic force microscopy*" Biomacromolecules 10: 2571-2576.

[45] Xiang Yang Liu et al. (2016) "*Fabrication of a uniaxial cellulose nanocrystal thin film for coassembly of single-walled carbon nanotubes*" RSC advances 42: 39396-39400.

[46] Revol J.F., Bradford H., Giasson J., Marchessault R.H., Gray D.G. (1992) "*Helicoidal self-ordering of cellulose microfibrils in aqueous suspension*" International journal of Biology and Macromolecules 14: 170-172.

[47] Orts W.J., Godbout L., Marchessault R.H., Revol J.F. (1998) "*Enhanced ordering of liquid crystalline suspensions of cellulose microfibrils: a small angle neutron scattering study*" Macromolecules 31: 5717-5725.

[48] Sacui I.A., Nieuwendaal R.C., Burnett D.J., Stranick S.J., Jorfi M. et al. (2014) "*Comparison of the properties of cellulose nanocrystals and cellulose nanofibrils isolated from bacteria, tunicate, and wood processed using acid, enzymatic, mechanical and oxidative methods*" Applied materials and interfaces 6: 6127-6138.

[49] Dong X. M., Revol J. F., Gray D. G. (1998) "*Effect of microcrystalline preparation conditions on the formation of colloidal crystals of cellulose*" Cellulose 5: 19-32.

[50] Ranby B.G. (1949) "*Aqueous colloidal solutions of cellulose micelles*" Acta Chemica Scandinava 3: 649-650.

[51] Aslanzadeh S. (2014) "*Pretreatment of cellulosic waste and high rate biogas production*" Doctoral thesis on resource recovery, University of Boras, Boras, 1-50.

[52] *http://www.sswm.info/content/biogas-settler* (Last access on 28/03/2017)

[53] Pavlostathis S. G., Giraldo-Gomez E. (1991) "*Kinetics of anaerobic treatment: a critical review*" Critical reviews in environmental control 21(5-6): 411-490.

[54] Gavala H. N., Angelidaki I., Arring B. K. (2003) "*Kinetics and modeling of anaerobic digestion process*" Advances in biochemical engineering and biotechnology 81: 57-93.

[55] Yadvika S., Sreekrishnan T.R., Khol, S., Rana V. (2004) "*Enhancement of biogas production from solid substrates using different techniques - A review*" Bioresource Technology 95: 1-100.

[56] Gerardi M.H. (2003) "*The microbiology of anaerobic digesters*" Wiley, Hoboken, 89-92.

[57] Deublein D., Steinhauser A. (2008) "*Biogas from waste and renewable resources: an introduction*" Wiley-VCH, Weinheim, 89-290.

[58] Bryant M. (1979) "*Microbial methane production: theoretical aspects*" Journal of animal science, Vol. 48, No. 1: 193-201.

[59] Smith P. (1966) "*The microbial ecology of sludge methanogenesis*" Developments in industrial microbiology, Vol. 7: 156-161.

[60] Conrad R. (1999) "*Contribution of hydrogen to methane production and control of hydrogen concentrations in*

methanogenic soils and sediments" FEMS Microbiology ecology, Vol. 28, No. 3: 193-202.

[61] Parawira W., Read J. S., Mattiasson B., Bjornsson L. (2008) "*Energy production from agricultural residues: high methane yields in pilot-scale two-stage anaerobic digestion*" Biomass and Bioenergy, Vol. 32, No. 1: 44-50.

[62] Claassen P. A. M., Lopez Contreras A. M., Sijtsma L. et al. (1999) "*Utilisation of biomass for the supply of energy carriers*" Applied microbiology and biotechnology, Vol. 52, No. 6: 741-755.

[63] Conrad R. (1999) "*Contribution of hydrogen to methane production and control of hydrogen concentrations in methanogenic soils and sediments*" FEMS Microbiology ecology, Vol. 28, No. 3: 193-202.

[64] Ntaikou I., Antonopoulou G., Lyberatos G. (2010) "*Biohydrogen production from biomass and wastes via dark fermentation: a review*" Waste and biomass valorization, Vol. 1, No. 1: 21-39.

[65] Schink B. (1997) "*Energetics of syntrophic cooperation in methanogenic degradation*" Microbiology and molecular biology reviews, Vol. 61, No. 2: 262-280.

[66] De Bok F. A. M., Harmsen H. J. M., Plugge C. M. et al. (2005) "*The first true obligately syntrophic propionate-oxidizing bacterium, Pelotomaculum schinkii sp. nov., co-cultured with Methanospirillum hungatei, and emended description of the genus Pelotomaculum*" International journal of systematic and evolutionary microbiology, Vol. 55, No. 4: 1697-1703.

[67] Verstraete W., Doulami F., Volcke E., Tavernier M., Nollet H., Roles J. (2002) "*The importance of anaerobic digestion for global environmental development*" Proceedings of the JSCE annual meeting: 97-102.

[68] Griffin M. E., McMahon K. D., Mackie R. I., Raskin L. (1998) "*Methanogenic population dynamics during start-up of anaerobic digesters treating municipal solid waste*

and biosolids" Biotechnology and bioengineering, Vol. 57, No. 3: 342-355.

[69] Karakashev D., Batstone D. J., Angelidaki I. (2005) "*Influence of environmental conditions on methanogenic compositions in anaerobic biogas reactors*" Applied and environmental microbiology, Vol. 71, No. 1: 331-338.

[70] Appels L., Baeyens J., Degreve J., Dewil R. (2008) "*Principles and potential of the anaerobic digestion of waste-activated sludge*" Progress in energy and combustion science 34: 755-781.

[71] Lindner J., Zielonka S., Oechsner H., Lemmer A. (2015) "*Effect of different pH-values on process parameters in two-phase anaerobic digestion of high-solid substrates*" Environmental technology 36 (1-4): 198-207.

[72] Sluiter A., Hames B., Ruiz R., Scarlata C., Sluiter J., Templeton D., Crocker D. (2011) "*Determination of structural carbohydrates and lignin in biomass - Laboratory analitycal procedure (LAP)*" National renewable energy laboratory.

[73] Mariotti F., Tome D., Patureau Mirand P. (2008) "*Converting nitrogen into protein - Beyond 6.25 and Jones' factor*" Food science and nutrition 48(2): 177-184.

[74] Santos M., Jimenez J. J., Bartolome B., Gomez-Cordoves C., Del Nozal M. J. (2003) "*Variability of brewer's spent grain within a brewery*" Food chemistry 80: 17-21.

[75] *https://secure.megazyme.com/Sucrose-Fructose-D-Glucose-Assay-Kit* (Last access on 29/03/2017)

[76] *http://www.sigmaaldrich.com/catalog/product/sigma/sa20?lang=it&region=IT* (Last access on 29/03/2017)

[77] Segal L., Creely J.J., Martin A. E., Conrad C. M. (1959) "*An empirical method for estimating the degree of cristallinity of native cellulose using the X-Ray diffractometer*" Textile research journal: 786-794.

[78] Xian-Zheng Yuan et al. (2014) "*Modeling anaerobic digestion of blue algae: stoichiometric coefficients of amino acids acidogenesis and thermodynamics analysis*" Water research 49: 113-123.

[79] Patricio Lopez Exposito et al. (2017) "*Laser reflectance measurement for the online monitoring of chlorella sorokiniana biomass concentration*" Journal of biotechnology 243: 10-15.

[80] Klamczynski A., Baik BK, Czuchajowska Z. (1998) "*Composition, microstructure, water imbibition, and thermal properties of abraded barley*" Cereal Chem 75: 677-685.

[81] Sullivan P., O'Flaherty J., Brunton N. (2009) "*Chemical composition and microstructure of milled barley fractions*" Eur Food Res Technol 230: 579-595.

[82] Pires E. J., Ruiz H. A., Teixeira J. A., Vicente A. A. (2012) "*A new approach on brewer's spent grains treatment and potential use as lignocellulosic yeast cells carriers*" Journal of agricultural and food chemistry 60: 5994-5999.

[83] Moser et al. (2015) "*Cellulose nanofiber testing*" BioResources 10 (2): 2360-2375.

[84] Fayyaz Ali Shah et al. (2014) "*Microbial ecology of anaerobic digesters: the key players of anarobiosis*" The scientific world journal Vol. 2014, ID 183752, 21 pages.

[85] Bayr S. (2014) "*biogas production from meat and pulp and paper industry by-products*" Jyvaskyla studies in biological and environmental science 280.

[86] Dangcong P., Qiting J. (1993) "*Anaerobic digestion of alkaline black liquor using an up-flow anaerobic sludge blanket reactor*" Journal of chemistry technology and biotechnology 58: 89-93.

[87] Fillandeau L., Balnpain-Avet P., Daufin G. (2006) "*Water, wastewater and waste management in brewing industries*" Journal of cleaner production 14: 463-471.

[88] Mussatto S. I., Dragone G., Roberto I. C. (2006) "*Brewers' spent grain: generation, characteristics and potential applications*" Journal of cereal science 43: 1-14.

[89] Ben-hamed U., Seddight H., Thomas K. (2011) "*Economic returns of using Brewery's spent grain in animal feed*" International journal of social, behavioral, educational, economic, business and industrial engineering Vol. 5, No. 2 43: 1-14.

[90] Enitan A. M., Adeyemo J., Kumari S., Swalaha F. M., Bux F. (2015) "*Chracterization of brewery wastewater composition*" International journal of environmental, chemical, ecological and geophysical engineering Vol. 9, No. 9.

[91] Xiaofeng Liu et al. (2016) "*Kinetics of methane production and hydrolysis in anaerobic digestion of corn stover*" Energy 102: 1-9.

[92] Mani S., Sundaram J., Das K.C. (2016) "*Process simulation and modelling: anaerobic digestion of complex organic matter*" Biomass and bioenergy 93: 158-167.

Ringraziamenti

Il primo ringraziamento va senza dubbio al Professor Alberto Bertucco e alla Dottoressa Elena Barbera che mi hanno seguito passo passo nello sviluppo di questa Tesi, offrendomi consigli preziosi e spronandomi a dare il massimo, sempre sicuri della buona riuscita dei miei sforzi.
Allo stesso modo ringrazio i componenti del gruppo "Celulosa y papel" della UCM di Madrid: senza l'aiuto di Luis, Cristina, Patricio, Noemí e Helen non sarei mai riuscito ad affrontare le difficoltà di un lavoro di ricerca così complesso, né avrei potuto passare dei mesi tanto felici ed appassionati.
Dopodiché vorrei ringraziare la mia famiglia, che più di tutti dimostra giornalmente di avere la più completa e cieca fiducia nella persona che loro stessi mi hanno aiutato a diventare: siete le parole dolci nel momento dello sconforto, il rimprovero in risposta alla tentazione dell'abbandono. Non potrei essere più fortunato.
A questo punto urge ringraziare gli amici: siete molti, siete vicini, siete lontani; ma ognuno di voi a suo modo mi fa sentire il suo affetto, ognuno di voi presta il proprio orecchio al racconto delle mie difficoltà e alla stessa maniera gioisce con me ad ogni possibile scusa per farlo. Questa Tesi la dedico a voi, che mi avete plasmato e fatto trovare il mio posto all'interno della società.
Infine vorrei ringraziare il mio ragazzo, Giovanni: gli ultimi mesi sono stati duri, ma nonostante la lontananza mai in vita mia ho sentito nei miei confronti un affetto tanto forte, un tale supporto, la più dedita presenza. Grazie per essere al mio fianco.